UC Santa Cruz

UC Santa Cruz Previously Published Works

Title

Structure and mechanism of human cystine exporter cystinosin.

Permalink

Journal

Cell, 185(20)

Authors

Guo, Xue

Schmiege, Philip

Assafa, Tufa

et al.

Publication Date

2022-09-29

DOI

10.1016/j.cell.2022.08.020

Peer reviewed

Structure and Mechanism of Human Cystine Exporter Cystinosin

Xue Guo[1,6], **Philip Schmiege**[2,6], **Tufa E. Assafa**[3,6], **Rong Wang**[2], **Yan Xu**[1], **Linda Donnelly**[2], **Michael Fine**[2], **Xiaodan Ni**[4], **Jiansen Jiang**[4], **Glenn Millhauser**[3,*], **Liang Feng**[1,7,8,*], **Xiaochun Li**[2,5,7,*]

[1]Department of Molecular and Cellular Physiology, Stanford University School of Medicine, Stanford, CA 94305, USA,

[2]Department of Molecular Genetics, University of Texas Southwestern Medical Center, Dallas, TX 75390, USA,

[3]Department of Chemistry and Biochemistry, University of California, Santa Cruz, CA 95060, USA,

[4]Laboratory of Membrane Proteins and Structural Biology, Biochemistry and Biophysics Center, National Heart, Lung, and Blood Institute, National Institutes of Health, Bethesda, MD 20892, USA,

[5]Department of Biophysics, University of Texas Southwestern Medical Center, Dallas, TX 75390, USA

[6]These authors contributed equally: Xue Guo, Philip Schmiege and Tufa E. Assafa

[7]These authors contributed equally: Liang Feng and Xiaochun Li

[8]Lead Contact

Summary

Lysosomal amino acid efflux by proton-driven transporters is essential for lysosomal homeostasis, amino acid recycling, mTOR signaling, and maintaining lysosomal pH. To unravel mechanisms of these transporters, we focus on cystinosin, a prototypical lysosomal amino acid transporter

DECLARATION OF INTERESTS
P.S., L.D., and X.L. have a provisional patent for the 3H5 variable sequence: Serial No. 63/366,972, entitled "Anti-Human, Cystinosin Antibodies and Methods of Use Thereof". The rest of the authors do not declare any conflict of interest.

INCLUSION AND DIVERSITY
One or more of the authors of this paper self-identifies as an underrepresented ethnic minority in science.

that exports cystine to the cytosol, where its reduction to cysteine supplies this limiting amino acid for diverse fundamental processes and controlling nutrient adaptation. Cystinosin mutations cause cystinosis, a devastating lysosomal storage disease. Here, we present structures of human cystinosin in lumen-open, cytosol-open, and cysteine-bound states, which uncover the cystine recognition mechanism and capture key conformational states of the transport cycle. Our structures, along with functional studies and Double Electron–Electron Resonance spectroscopic investigations, reveal the molecular basis for the transporter's conformational transitions and protonation switch, show conformation-dependent Ragulator-Rag complex engagement, and demonstrate an unexpected activation mechanism. These findings provide molecular insights into lysosomal amino acid efflux and a potential therapeutic strategy.

Graphical Abstract
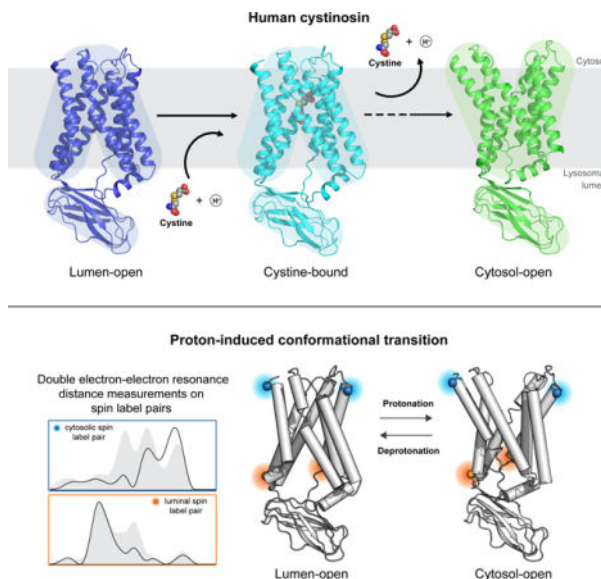
In Brief:

Structural and biophysical studies of human cystinosin reveal molecular mechanisms and conformational dynamics in proton-coupled lysosomal amino acid transport.

Introduction

Forty years ago, pioneering studies demonstrated carrier-mediated lysosomal cystine transport and its connection to the defect that causes cystinosis (Gahl et al., 1982; Jonas et al., 1982; Gahl, 1987), a devastating lysosomal storage disease in which abnormal cystine buildup (Schneider et al., 1967; Gahl et al., 1982; Jonas et al., 1982; Gahl et al., 2002) forms intracellular crystals that gradually damage cells and organs (Cherqui and Courtoy, 2017; Gahl et al., 2002). Since then, other lysosomal membrane transport systems (and linked lysosomal storage diseases) have been discovered, revealing the rich and dynamic roles membrane transport proteins play in lysosomal biology.

Lysosomal efflux transporters export (into the cytosol) the metabolites resulting from lysosomal degradation of macromolecules. These transporters usually are driven by the proton gradient across the lysosomal membrane, and their transport activities are thus tightly coupled to V-ATPase activity, which sets the acidic pH of the lysosomal lumen (Abu-Remaileh et al., 2017; Bissa et al., 2016). Accumulating evidence suggests lysosomal amino acid transporters play critical roles maintaining cellular homeostasis and modulating signaling hubs (Abu-Remaileh et al., 2017; Jouandin et al., 2022; Liu et al., 2012; Wyant et al., 2017). Yet despite decades of biochemical, functional, genetic, and physiological studies, the transport mechanisms of proton-coupled lysosomal amino acid efflux transporters remain unclear.

In proliferating cells, lysosomal concentrations of amino acids are generally lower than whole cells, with one remarkable exception: cystine, the oxidized dimeric form of cysteine. Cystine is ~ 30-fold more concentrated in lysosomes compared to the cytosol (Abu-Remaileh et al., 2017), where it is quickly reduced into cysteine. Lysosomal cystine serves as the predominant reservoir for intracellular cysteine, the least abundant and often limiting amino acid. Cystine efflux is governed by the proton-coupled transporter cystinosin, which regulates the cytosolic level of cysteine for diverse fundamental processes, such as antioxidant glutathione synthesis and transfer RNA thiolation. During fasting, lysosomal cystine efflux mediated by cystinosin controls the cellular response to nutrient restriction through limiting TORC1 activity (Jouandin et al., 2022). Thus, cystinosin is crucial both for maintaining cystine and cysteine availability, and for regulating the response of signaling pathways to nutrient status (Andrzejewska et al., 2016; Jouandin et al., 2022; Kalatzis et al., 2001). Cystinosin dysfunction leads to the accumulation of cystine inside lysosomes and causes cystinosis (Gahl et al., 1982; Gahl et al., 2002; Jonas et al., 1982; Town et al., 1998).

Cystinosin is the founding member of the PQ-loop transporter family, whose members are characterized by a pair of highly conserved proline-glutamine motifs. These transporters share limited sequence similarity with transporters of known structure (Feng and Frommer, 2016; Saudek, 2012). They shuttle amino acids across the lysosomal membrane, playing essential roles in supporting lysosome functions, maintaining amino acid homeostasis, and transducing nutrient signaling (Amick et al., 2020; Andrzejewska et al., 2016; Jezegou et al., 2012; Leray et al., 2021; Liu et al., 2012; Lobry et al., 2019; Talaia et al., 2021; Zhang et al., 2017). Cystinosin is well conserved across species (Figure S1) and unique for its strict substrate selectivity for cystine (Ruivo et al., 2012). Other known lysosomal amino acid transporters, including other PQ-loop transporters, generally recognize a range of amino acids with overlapping properties (Bröer and Bröer, 2017). For example, PQLC2, mediates lysosomal efflux of cationic amino acids such as arginine, lysine, histidine, and ornithine (Jezegou et al., 2012; Talaia et al., 2021). Yet the molecular determinants that underlie substrate selectivity and the transport cycle of cystinosin—or any other PQ-loop transporters —have remained obscure.

Another key feature of cystinosin is transport coupling. PQ-loop transporters belong to the MtN3 clan (superfamily), which encompasses a diverse array of membrane proteins, such as SWEET sugar transporters and KDEL receptors (KDELR) (Bräuer et al., 2019; Saudek, 2012; Tao et al., 2015). Yet while SWEETs mediate passive transport of sugar through

facilitated diffusion (Chen et al., 2010a), cystinosin is a symporter that couples the transport of cystine with proton at a 1:1 ratio (Ruivo et al., 2012). How a proton is coupled to cystine transport is not well understood. More broadly, the fundamental question of how the transport rate of a transporter is regulated remains poorly understood. Answering this question is crucial for understanding transport mechanisms and for manipulating transport activity in translational applications. In particular, many medical and biotechnological applications would benefit from enhancing transport activity, but our limited understanding of the rate limiting step(s) in a transport cycle has constrained our ability to devise applicable modifying strategies.

Here we report structures of human cystinosin in lumen-open, cytosol-open, and cystine-bound states by crystallography and cryo-EM. These structures, together with functional characterizations and Double Electron-Electron Resonance (DEER) analyses, define the architecture of the PQ-loop family, provide insights into the mechanism of cystine transport, reveal an unexpected activation mechanism, and advance our knowledge on the pathogenesis of cystinosis and mTOR signaling.

Results

Structures of cystinosin

Given purified human cystinosin is refractory to crystallization, we conducted systematic alanine scanning mutagenesis on every residue in the transmembrane domain (TMD) to identify thermostabilizing mutations. Introducing one such mutation, N301A, together with a nanobody P10 as a crystallization chaperone, yielded crystals in lipidic cubic phase that diffracted X-rays to 3.4 Å resolution (Figure S2 and Table S1). Overall, cystinosin resembles a Sarracenia-like structure with the luminal N-terminal domain (NTD) protruding from the TMD (Figure 1A). Cystinosin's NTD adopts a β-sandwich fold, resembling an immunoglobulin domain. The TMD contains seven transmembrane (TM) helices. The N-terminal TMs 1–3 and C-terminal TMs 5–7 form two similar triple helix bundles (THB) that are connected by an inversion linker helix, TM4 (Figure 1B). A large solvent-accessible cavity opens on the luminal side and extends deep into the transporter, indicating a lumen-open conformation.

In parallel, we pursued cryo-EM studies to investigate cystinosin's main conformational states. Cystinosin-binding antibody 3H5 fragments (Fab[3H5]) were generated to provide a fiducial mark to facilitate particle alignment. This allowed us to determine structures of wild-type (WT) human cystinosin in two conformational states (Figure S3 and Table S2). Cystinosin-Fab[3H5] purified at pH 7.5 yielded a lumen-open conformation structure at 3.4 Å resolution, which superimposes well onto the crystal structure (Figure 1C–D). Our structures, derived with two distinct techniques, cross-validate each other. In contrast, cystinosin-Fab[3H5] purified at pH 5.0 yielded a 3.2 Å resolution cytosol-open structure with pronounced conformational changes in the TMD that result in a large central cavity accessible from the cytosol (Figure 2A–B).

Structural comparisons with other transporters revealed that cystinosin's NTD shares a similar fold to that of Niemann-Pick protein C2 (Li et al., 2016) (Figure S4A). Cystinosin's

TMD adopts a similar fold to eukaryotic SWEET sugar transporters and KDEL receptors, despite their low sequence similarity (~ 19% and ~ 23% identity to SWEET (PDB: 5CTG) and KDELR (PDB: 6I6B), respectively) and divergent functions (Bräuer et al., 2019; Han et al., 2017; Tao et al., 2015) (Figure S4C–D). This supports previous predictions that they can be grouped in the same membrane protein superfamily (Saudek, 2012). The AlphaFold model (AF-O60931-F1) aligns well with the cytosol-open conformation (root mean square deviation, r.m.s.d. = 0.8 Å), while alignment with the lumen-open conformation shows significant differences (r.m.s.d. = 2.9Å) (Figure S4E). This comparison illustrates both the promise and limitation of this prediction algorithm.

NTD-TMD interaction

The NTD is unique to cystinosin among PQ-loop transporters. Removing the NTD reduced cystine transport activity by ~ 70% in a cell-based uptake assay (Figure 2C) and severely impaired the expression and stability of cystinosin (Figure S4H and S4J), suggesting an important structural role. This is consistent with early discoveries that an internal deletion in the NTD is linked to cystinosis and causes protein misfolding (Kalatzis et al., 2004; Nevo et al., 2017). The NTD makes direct—but loose—contact with the TMD through two interfaces (Figure 2D). At one interface, Q96 on NTD interacts with residues on the loop connecting TM6 and TM7 (L6–7), helping anchor the NTD in place. At the other interface, NTD residues contact the luminal loop between TM2 and TM3 (L2–3). The specific residues at this interface differ in the lumen-open and cytosol-open conformations as L2–3 undergoes an inward movement relative to L6–7 between these two conformations. Thus, it is conceivable that the NTD might affect the conformational switch of the TMD and regulate transport activity. Indeed, the NTD-TMD interface is enriched with conserved residues of the NTD (Figure S4B). Mutating NTD residues on the NTD-TMD interface impacted the transport activity: substitution Q96A severely impaired cystine uptake (Figure 2C), and several others—S64A, K65A, G95A, and T98A—reduced transport activity to varying degrees (Figure S4G). Among these residues, G95 is adjacent to Q96, perhaps supporting its proper configuration. T98 helps to reposition L2–3 upon the luminal gate's opening. K65 forms electrostatic interaction with L6–7, and its neighboring residue S64 helps to position K65. Several other mutations had only modest effects on transport activity (Figure 2C and Figure S4G). Together, our structural observations and functional analyses suggest NTD-TMD communication is important for cystinosin function.

Substrate translocation pathway and cystine binding

The central cavities of the lumen- and cytosol-open structures overlap in a region of the transporter closer to the cytosolic side. This area of overlap may indicate a potential substrate binding site that is alternately exposed to either side of the membrane during the transport cycle. Numerous disease-causing mutations have been identified in cystinosin (David et al., 2019), and they are enriched in these central cavity-lining residues (Figure 3D), consistent with their important functional roles (Figure S4G).

To gain insights into how cystinosin specifically recognizes cystine, we determined the cryo-EM structure of cystine-bound cystinosin at 3.4 Å resolution (Figure S3G–J and Table S2). An elongated extra density was found at the bottom part of the central cavity. This

density was absent in the apo structures (determined without cystine), and the shape matches cystine (Figure 3A). Thus, we attribute this density to cystine. This structure superimposes well onto that of the apo lumen-open state (Figure 3B), representing a substrate-bound, lumen-open state.

Multiple cavity-lining residues interact with the amino acid moieties on both ends of cystine (Figure 3C). One amino acid moiety occupies a central region of the binding pocket and interacts with K273, K280, Y281, and D305; the other inserts into the bottom of the binding pocket and interacts with N166 and N301. W138 forms a hydrogen bond with D305, which stabilizes its conformation to interact with cystine, and is in close range to cystine. F142 and F170 are also in range to form hydrophobic interactions with cystine around its disulfide bridge, in a similar fashion as that of other soluble cystine-binding proteins (Bulut et al., 2012; Lu et al., 2014). Mutating K273, K280, D305, W138, N166 and F142 abolished cystine transport, while mutating Y281, N301 and F170 substantially reduced transport activity (Figure 2C), corroborating our structural observations. Notably, K280 and D305 are clinically relevant as mutation of either residue causes cystinosis (Kalatzis et al., 2004).

Unlike many other amino acid transporters that can transport multiple amino acids with similar properties, cystinosin has a tight substrate selectivity for cystine over all canonical amino acids (Ruivo et al., 2012). Our structures reveal a narrow and elongated cavity that fits well with the shape of cystine (Figure 3A). Importantly, cystinosin makes specific interactions with the amino and carboxyl groups on both ends of cystine, providing a "molecular ruler" that dictates the selectivity for the dimeric cystine over the monomeric canonical amino acids.

Luminal and cytosolic gates

During the transport cycle, the luminal and cytosolic gates control the access of the substrate binding pocket to either side of the membrane and thus play central roles in the alternating transport mechanism. Comparing cystinosin structures in lumen-open vs. cytosol-open conformations reveals key elements of the luminal and cytosolic gates. In the cytosol-open conformation, the central substrate translocation pathway is sealed from the lysosomal lumen by a luminal gate formed by a network of interacting residues, Y134, D205, and K335 (Figure 4A). D205 on TM3 forms a salt bridge with K335 on TM7, which brings the luminal side of N-THB and C-THB in close proximity. In addition, Y134 interacts via hydrogen bonding with D205, which helps to stabilize its interaction with K335. These interactions are specific to the cytosol-open conformation and are absent in the lumen-open conformation (Figure 4B). The formation of the luminal gate is associated with the repositioning of L2–3. In association with the inward tilting of TM2 and TM3 at the luminal side, L2–3 runs across the center of the mouth of the translocation pathway and shields the vestibule from the lysosomal lumen. In this conformation, L2–3 interacts with R114 on NTD and Q319 on TM6 from C-THB, which may help stabilize the closed luminal gate (Figure 2D and Figure 4A).

Substituting Y134, D205 and K335 alanine abolished or severely impaired cystine transport activity (Figure 4C), as did the more conservative substitutions D205N or Y134F. This suggests the importance of the interaction network of the luminal gate. In addition, the

Q319A mutation substantially reduced cystine uptake, pointing to an important role of residues that facilitate closing of the luminal gate.

In the lumen-open conformation, the cytosolic gate seals the translocation pathway from the cytosol. The glutamine residues of the signature PQ motifs on both THBs are key in closing the cytosolic gate (Figure 4B). Q145 of the first PQ motif forms a hydrogen bond with backbone amides on the cytosolic loop that connects TM5 and TM6 (L5–6). The bulky sidechain of W297 on L5–6 interacts with Q284 of the second PQ motif through amide-π stacking (Figure 4B). Q284 is also in range to form a hydrogen bond with the backbone oxygen on the cytosolic loop L1–2. Thus, the interaction network mediated by Q145 and Q284 brings L1–2 on N-THB and L5–6 on C-THB in close proximity at the entrance of the central cavity, shielding the cavity from the cytosolic solvent. In addition, W297 on L5–6 inserts its indole ring into the central cavity, which helps occlude the translocation pathway.

To probe the roles of the key residues that form the cytosolic gate, we assayed the effect of Q145A and Q284A. Both variants showed clearly enhanced cystine uptake activity with a reduction in the Michaelis constant (K_m) and an increase in the maximum velocity (V_{max}) (Figure 4D). These gain-of-function mutations reveal the important functional impact of weakening cytosolic gate formation by breaking the interactions mediated by Q145 or Q284. Intriguingly, this has the opposite effect to weakening the luminal gate formation (Figure 4C).

Notably, besides mediating cytosolic gate formation, the PQ motifs also facilitate conformational transitions. In transition from the lumen-open to cytosol-open conformation, the cytosolic portion of TM5 undergoes a large outward movement around the kink at P283 of the second PQ motif. Concomitantly, the cytosolic portion of TM1 also moves outward around a kink near P144 (Figure S4F). These conformational changes lead to a pronounced outward movement of L1–2 and L5–6 to unblock the translocation pathway and significantly enlarge the cytosolic entrance. Thus, the PQ motifs are central to linking the conformational switch to cytosolic gate formation, revealing the functional significance of the signature PQ motif that defines this family of transporters.

Conformational transitions

Transporters typically oscillate between outward (lumen)-facing and inward (cytosol)-facing conformations to achieve alternating access transport. To gain insights into cystinosin's conformations and the role of gates in shaping conformational states, we carried out DEER spectroscopic studies, which measure the distance distribution of spin-labeled cysteine pairs that were introduced into a cysteine-free background of cystinosin. Two pairs of reporter positions were chosen to monitor cystinosin's conformational states: the cytosolic pair at the cytosolic end of TM3 and TM7 and the luminal pair at the luminal end of TM3 and TM6 (Figure 5A). Both pairs are expected to undergo significant distance changes between lumen- and cytosol-open conformations based on our structures. For WT cystinosin, both pairs show distance distributions that include features of the simulated distance distributions based on both lumen-open and cytosol-open structures (Figure 5B and Figure S5A–C), indicating that both cytosol-open and lumen-open conformations are populated in cystinosin in solution.

Substitutions of key luminal gate residues—D205N, K335A and Y134A—shifted the distance distribution of the cytosolic pair towards the shorter distance, indicating a predominantly closed conformation at the cytosolic side (Figure 5C and Figure S5A–C). For the luminal pair, all these mutations led to a predominantly long-distance distribution, indicating mostly an open conformation at the luminal side. A closed conformation on the cytosolic side in conjunction with an open conformation on the luminal side, matches well with a transporter in a lumen-open conformation. Therefore, the luminal gate mutations of cystinosin favor the lumen-open conformation. In contrast, cytosolic gate mutations, Q145A or Q284A, shifted the distance distribution of the cytosolic pair towards the longer distance and the luminal pair towards the shorter distance (Figure 5D and Figure S5A–C), consistent with structural features of cystinosin in a cytosol-open conformation. Thus, cytosolic gate mutations favor a cytosol-open conformation. These results suggest interactions at either the luminal gate or the cytosolic gate can maintain or drive closure of the respective gate and play critical roles in conformational switch of cystinosin.

pH-dependent conformational changes

Cystinosin is a proton-coupled symporter that harnesses the lysosomal proton gradient to facilitate cystine efflux (Kalatzis et al., 2001; Ruivo et al., 2012). In a cell-based uptake assay where cystinosin was redirected to plasma membrane, the uptake activity increases with a decrease of extracellular pH (Kalatzis et al., 2001). To investigate how a proton is coupled to the conformational switch of cystinosin, we monitored distance distributions across ten titration steps between pH 5.0 and 9.5 (Figure 6A–B and Figure S5D–F). At a high pH, the long-distance distribution of the luminal pair and the short-distance distribution of the cytosolic pair indicates cystinosin is predominantly in a lumen-open conformation. As the pH decreased, the distance distribution of the cytosolic pair shifted towards the long distance while that of the luminal pair shifted towards the short distance, suggesting that protonation of cystinosin favors cytosol-open conformations. At a low pH, cystinosin is predominantly in a cytosol-open conformation. During the titration, the distance distributions of the luminal and cytosolic pairs showed an overall inverse correlation. This is consistent with the negatively coupled luminal and cytosolic gates, which is important to achieve alternating access transport.

To pinpoint the molecular determinant responsible for the proton-induced conformational switch, we examined all acidic residues along the translocation pathway, including D205, D305 and D346. Each aspartate was mutated to asparagine to mimic the protonated state, and their distance distributions were measured at pH 5.2 (to favor protonation) and pH 7.4 (to favor deprotonation) (Figure 6C–D and Figure S5A–C). D205N substitution caused opening of the luminal side and closing of the cytosolic side in a pH-independent manner, which are opposite to proton-induced changes observed in WT. Given the critical role of D205 in the luminal gate formation, D205N should impair the luminal gate formation and favor the lumen-open conformation.

Asparagine substitution of D305, a previously proposed proton-binding site, showed a pH-dependent conformational switch similar to WT. In both cases, lowering the pH shifted the population towards the cytosol-open conformation, although D305N was biased toward

a lumen-open conformation at pH 7.4. Thus, D305 does not seem to mediate the pH-dependent conformational switch directly, despite its importance for proton transport (Ruivo et al., 2012). Neutralizing D346 abolished the pH-dependent conformational switch, as shown by nearly identical distance distributions at both pH values. Importantly, distance distributions of D346N at pH 7.4 predominantly show the long distance on the cytosolic side and short distance on the luminal side, which recapitulates the distance distributions of WT at pH 5.2. Hence, we postulate that D346 is a key protonation site for the proton-dependent conformational transition of cystinosin.

To probe cystinosin's conformation under a condition that better mimics the lysosomal environment, we aimed to carry out DEER studies on cystinosin reconstituted into liposomes with asymmetric pH across the membrane. Given that cystinosin reconstituted into liposomes yielded a mixed orientation (Figure S6D), we developed a strategy to release spin labels on the liposome exterior with the mild and membrane-impermeable reducing reagent TCEP (Cline et al., 2004; Deutschmann et al., 2022), which breaks the spin label disulfide attachment. As a result, subsequent to background correction, only proteins with spin labels on the liposome interior are EPR DEER detectable (Figure S6F). Under our experimental conditions, the reconstituted liposomes showed a proton gradient across the membrane (Figure S6B–C) with negligible TCEP permeability (Figure S6E). Continuous wave electron paramagnetic resonance (CW-EPR) kinetic studies showed a bi-exponential release of free spin labels by TCEP (Figure S6G–H), indicating that TCEP preferentially removed spin labels outside liposomes.

We measured the distance distributions of the luminal spin label pair inside liposomes under a lysosome-like environment (pH 5.2 'inside' and pH 7.4 'outside'). For WT cystinosin, we observed distance distributions representative for both lumen-open and lumen-closed states, indicating the co-existence of more than one major conformational state under physiological conditions (Figure S6I). In a control experiment, WT cystinosin with symmetrical pH inside and outside of liposomes undergoes pH-induced conformational transitions and favors the cytosol-open state at a low pH (Figure S6A), recapitulating observations on samples in micelles. Compared with the symmetric pH 7.4 condition, the lower luminal pH experienced by WT cystinosin resulted in a decrease in the long-distance distribution and an increase in the short-distance distribution of the luminal reporter pair, suggesting the lower luminal pH favors a closed conformation at the luminal side. The direction of the shift of distance distribution matches with that derived from lowering pH symmetrically, while the degree of the shift is less. We also examined the luminal distance distributions of three key D-to-N mutants under the same pH gradient (Figure S6I). D305N shows a mixed population of long- and short- distance distributions. In contrast, D346N and D205N show predominantly short- and long-distance distributions, respectively, the same as what we observed in micelles with a uniform pH. These results are consistent with observations on samples in micelles, corroborating these residues' proposed roles in shaping conformational transitions.

Cystinosin and the Ragulator-Rag complex interaction

Cystinosin regulates the mTOR pathway through its cystine transport activity and binding to the Ragulator-Rag complex (Andrzejewska et al., 2016; Jouandin et al., 2022), but the

molecular basis for the engagement between cystinosin and the Ragulator-Rag complex is unclear. An intriguing observation was that the N288K substitution suppresses cystinosin's interaction with the Ragulator-Rag complex (Andrzejewska et al., 2016) (also see Figure 7A). Based on our structures, N288 is located near the cytosolic end of TM5 and is not on the exterior surface of the protein. Conceivably, N288K may induce structural/ conformational changes in cystinosin and impact its interaction with the Ragulator-Rag complex. We thus determined the cryo-EM structures of N288K at pH 5.0 and pH 7.5 (3.0 and 3.1 Å resolution, respectively) (Figure 7B and Figure S7). It turns out that N288K adopts a cytosol-open conformation at both pH values, which matches very closely to the cytosol-open structure of WT at pH 5.0 (Figure 7B). Notably, the residue N288K forms a π-cation interaction with F349 to confine the cytosolic gate to an open state (Figure 7B). These results suggest that N288K favors the cytosol-open conformation. Corroborating this, our DEER studies reveal that N288K predominantly shows a long distance for the cytosolic reporter pair and a short distance for the luminal reporter pair at both pH values (Figure 6E–F).

We noted that, while N288K abolished cystine transport (Figure S4G), other variants that favor cytosol-open conformation, such as D346N, caused gain of function with enhanced activity (Figure 4C). This raises the question whether the N288K variant is trapped in a cytosol-open conformation. We thus carried out cysteine accessibility studies on reporter cysteine residues that were introduced at locations accessible in either lumen- or cytosol-open conformations (Figure 7C). For N288K, the cytosolic reporter cysteine (Y281C) was fully accessible, but the luminal reporter (S312C) only showed around background-level accessibility (Figure 7D). This suggests the N288K variant is trapped in a cytosol-open conformation and its ability to go through the transport cycle is crippled, which explains its loss of function. In contrast, for D346N (gain-of-function, favors cytosol-open), D205N (loss-of-function, favors lumen-open), and D305N (loss-of-function, pH-dependent conformations), both cytosolic and luminal cysteine reporters were accessible (Figure 7D). Our co-IP results confirmed that N288K disrupts cystionosin's interaction with V-ATPase, RagA/C, and p18 (a component of Ragulator) (Andrzejewska et al., 2016); in contrast, D205N, D305N, D346N showed much less pronounced effects on the interaction (Figure 7A). These results suggest that cystinosin trapped in a cytosol-open conformation does not interact with the Ragulator-Rag complex and conformational state(s) other than cytosol-open is likely required for recruitment of the Ragulator-Rag complex to regulate mTOR signaling. Elucidating the exact nature of this interaction awaits further work.

Discussion

Our structural and biophysical studies provide a molecular blueprint for mechanistic interpretation of disease-causing mutations in cystinosis. Many mutations line the substrate translocation pathway, and mutations that affect state transitions or protonation also underlie cystinosis. We also found two variants (G337R and L338P) that may cause protein-folding problems (Figure S4J), as they replace a glycine or introduce a proline.

Between the two configurations (3- and 7-TM) of the MtN3 clan, the 3-TM transporters are better characterized structurally (Feng and Frommer, 2016; Latorraca et al., 2017; Lee et al.,

2015; Wang et al., 2014; Xu et al., 2014). Previously, only the inward-open structures were captured for the 7-TM transporters (Han et al., 2017; Tao et al., 2015). Our work reveals the first outward (lumen)-open structure for 7-TM transporters and delivers significant insights into their transport cycle. Our cystinosin structures also represent the first for the PQ-loop family. As their name implies, the PQ-loop transporters possess a pair of highly conserved proline-glutamine repeats that were thought to be in loop regions. Our structures, however, reveal that the PQ motifs settle in the transmembrane helices TM1 and TM5 and play key roles in conformational transitions. This presents an interesting parallel to SemiSWEET, which is a symmetrical THB homodimer. In SemiSWEET, a PQ motif on each THB controls the conformational transition in an identical fashion (Feng and Frommer, 2015; Lee et al., 2015; Xu et al., 2014). In contrast, cystinosin's two PQ motifs operate asymmetrically but cooperatively, which might allow more sophisticated regulation of the conformational switch. Eukaryotic SWEET contains conserved prolines at comparable positions (Tao et al., 2015) but lacks glutamine residues, suggesting a distinct gating mechanism. Interestingly, KDELR, the receptor that mediates ER protein retrieval, adopts a similar architecture to cystinosin except that it retains only one PQ motif (Figure S4C). This difference might conceivably contribute to its inability to undergo the full conformational switch required for transport, thus facilitating its function as a receptor to retrieve ER proteins (Bräuer et al., 2019). These structural comparisons reveal shared features and distinctions among PQ-loop, SWEET, SemiSWEET and KDELR (Saudek, 2012), and they provide valuable information for understanding how varied THB construction supports diverse functions with distinct mechanisms.

Oscillating between outward- and inward-open conformations is fundamental for transporters to fulfill their transport functions. Besides revealing cystinosin's distinct states, our studies identified molecular determinants for transitions between lumen- and cytosol-open conformations. The luminal gate and the cytosolic gate both fulfill two critical functions: shielding the central substrate binding pocket from solution when they are closed and driving conformational state transitions. Disrupting gate interactions favors opening of the respective gate. Unexpectedly, we found that disrupting luminal and cytosolic gates produced opposite functional consequences: luminal gate mutations abolished or substantially reduced transport activity while cytosolic gate mutations enhanced transport activity. This implies the relative strength of the interactions at the outer and inner gates dictates transport kinetics. Moreover, these observations suggest that a facile transition to the cytosol-open conformation or an increased dwelling time in this conformation helps increase the transport activity, pointing to the rate limiting step(s) of the transport cycle. Altogether, changes in the relative strength of luminal and cytosolic gate interactions can facilitate or hinder the transition to the cytosol-open conformation, thus dictating transport kinetics. Consistent with this, the D346N substitution, which presumably mimics a protonated cystinosin, also favors the cytosol-open conformation and increases the transport activity (Figure 4C), further supporting the correlation between increased cytosol-open population and enhanced transport activity. These results suggest an important role for protonation in the transport of cystine, which raises the question whether other lysosomal transporters engage protons through a similar mechanism given their typical proton dependence. Interestingly, gate mutations in *Ec*SemiSWEET can increase or decrease

transport activity, but in an opposite manner to cystinosin: extracellular gate mutations (equivalent to the luminal gate of cystinosin) result in increased activity (Lee et al., 2015). This is probably due to different relative energy levels of conformational states and/or mechanisms of rate-limiting steps. These results suggest that modifying the relative stability of specific conformational states through gate mutations might be a more generally applicable mechanism to regulate transport activity.

Finally, our findings on a mechanism for substantially increasing transport activity suggest it may be possible to enhance cystinosin's transport activity by developing conformation-selective small molecules or biologics that favor a cytosol-open conformation. This points to a potential therapeutic strategy to alleviate the crippled cystine transport that underlies cystinosis. Similarly, targeting the conformational state of a rate-limiting step in a variety of other transporters may offer an applicable strategy to enhance their transport activity for important mechanistic and translational applications.

Limitations of the Study

Our studies show that pH induces conformational changes in cystinosin and revealed that protonation of specific aspartate residues may shift the equilibrium to facilitate transport. Nonetheless, the proton translocation pathway awaits elucidation, and the exact mechanism of how a proton is coupled to cystine translocation represents another exciting future direction. While we have captured the lumen-open and cytosol-open conformations, other conformational states, e.g., occluded structures, are needed to reach a comprehensive understanding of the transport cycle. Further, although we have gained interesting insights into the interaction between cystinosin and the Ragulator-Rag complex, we still need to identify the nature of interaction and how it is integrated into mTOR signaling to better understand the cross-talk between amino acid efflux and cellular signal transduction.

STAR★METHODS

RESOURCE AVAILABILITY

Lead contact—Further information and requests for resources and reagents should be directed to and will be fulfilled by the Lead Contact, Liang Feng (liangf@stanford.edu).

Materials availability—Unique reagents generated in this study are available with a completed materials transfer agreement.

Data and code availability

- The 3D cryo-EM density maps have been deposited in the Electron Microscopy Data Bank under the accession numbers 27489, 27488, 27490, 27492, and 27493. Coordinates for the cryo-EM structures and crystallographic coordinates and structural factors have been deposited in the Protein Data Bank under the accession numbers 8DKI, 8DKE, 8DKM, 8DKW, 8DKX, and 8DYP. All other data is available from the corresponding authors upon reasonable request.

- This paper does not report original code.

- Any additional information required to reanalyze the data reported in this paper is available from the lead contact upon request.

EXPERIMENTAL MODEL AND SUBJECT DETAILS

Sf9 insect cells were grown at 27 °C, with shaking at 120 rpm in ESF 921 medium (Expression Systems no. 96-001). HEK293S cells were maintained at 37 °C under 8% CO_2, with shaking at 130 rpm in FreeStyle™ 293 expression medium (Gibco no. 12338018) supplemented with 2% FBS. HEK293T cells were maintained at 37 °C with 5% CO_2 in high glucose DMEM (Gibco) with 10% FCS, 1% L-glutamine and 1% Penicillin-Streptomycin. The NIH/3T3 cells were maintained in high glucose DMEM (Gibco) with 10% newborn calf serum and 1% Penicillin-Streptomycin at 37 °C under 8.8% CO_2. For antibody production, hybridomas were initially cultured in plates at 37 °C under 8% CO_2 in HAT (hypoxanthine-aminopterin-thymidine) medium. After subcloning, 3H5 producing hybridomas were cultured in HT (hypoxanthine-thymidine) medium in roller bottles at 37 °C under ambient CO_2 at a speed of 2.5 rpm. *E.coli* BL21 (DE3) was cultured and induced at 37 °C using isopropyl-b-D-thiogalactopyranoside (IPTG) when OD_{600} reached 0.6.

METHOD DETAILS

Protein expression and purification—For crystallization studies, the sequence encoding residues 24–362 of human cystinosin (GenBank: AAF43102.1) was cloned into a modified pEG-BacMam vector with a haemagglutinin (HA) signal sequence followed by a maltose binding protein (MBP) tag at the N terminus and a GFP-8xHis tag at the C-terminus. The optimized variant contained a thermostabilizing mutation N301A, and mutation of glycosylation sites (N36A, N41A, N51A, N66A, N84A, N104A and N107A) in the NTD. Recombinant protein was expressed using baculovirus-mediated transduction of HEK293S cells (Goehring et al., 2014). In brief, baculoviruses were generated using *Spodoptera frugiperda* Sf9 insect cells (Expression Systems no. 94-001S). HEK-293S GnTI⁻ cells (ATCC no. CRL-3022) were infected with baculoviruses at a density of 3.0×10^6 cells per ml. After incubation at 37 °C for 16 hours, the culture was supplemented with 10 mM sodium butyrate, and transferred to 30 °C for another 48 hours before collection. Pelleted cells were washed with a hypotonic buffer (20 mM Tris-HCl pH 8.0 with a cocktail of protease inhibitors and DNase I). The crude membrane was homogenized by brief sonication in lysis buffer (20 mM Tris-HCl pH8.0, 150 mM NaCl, a cocktail of protease inhibitors and DNase I), then solubilized by adding 1% (w/v) lauryl maltose neopentyl glycol (LMNG) (Anatrace) and 0.1% (w/v) cholesteryl hemisuccinate (CHS) (Anatrace). Following centrifugation, recombinant cystinosin was isolated from the supernatant by HisPur cobalt resin (ThermoScientific). The N-terminal MBP and C-terminal GFP-8xHis tag were removed by 3C protease digestion. Protein samples were further purified by size-exclusion chromatography (SEC) on a Superdex 200 increase column (Cytiva) in SEC buffer containing 20 mM HEPES pH7.4, 150 mM NaCl, 0.002% LMNG, and 0.0002% CHS.

For cryo-EM studies, full-length human cystinosin-LKG (GenBank: AAH32850.1) was cloned into pEG-BacMam with a C-terminal Flag tag. The N288K mutant was generated using two-step PCR. The protein was expressed using baculovirus-mediated transduction of mammalian HEK-293S GnTI⁻ cells (ATCC no. CRL-3022) grown at 37 °C for 48 hours

post transduction. Cells were disrupted by sonication in lysis buffer (20 mM HEPES pH 7.5, 150 mM NaCl, 1 mM PMSF and 5 μg/mL leupeptin). After low-speed centrifugation, the supernatant was incubated with 1% (w/v) n-Dodecyl-β-D-Maltopyranoside (DDM, Anatrace) at 4 °C for 1 hour. The lysate was clarified by another centrifugation, and the resulting supernatant was loaded onto a Flag-M2 affinity column (Sigma-Aldrich). The resin was washed twice with wash buffer containing 20 mM HEPES pH7.5, 150 mM NaCl, and 0.02% DDM. The protein was eluted by wash buffer with 100 μg/mL 3×Flag peptide. The eluate was then concentrated and purified by SEC on a Superdex 200 Increase column (Cytiva). SEC buffer containing 20 mM HEPES pH7.5, 150 mM NaCl, and 0.06% (w/v) Digitonin (ACROS Organics) was used to obtain the apo lumen-open conformation and the N288K mutant at pH 7.5, while SEC buffer containing 20 mM sodium acetate pH5.0, 150 mM NaCl, and 0.06% (w/v) Digitonin was used to obtain the apo cytosol-open conformation and the N288K mutant at pH 5.0. To prepare cystine-bound cystinosin, protein samples were purified similarly with minor changes. 100 mM cystine stock was made in 1 M HCl due to its low solubility in neutral pH conditions. Buffers were supplemented with 1mM cystine immediately prior to use, yielding a final pH of ~7.0. Cells were sonicated in lysis buffer containing 20 mM HEPES pH8.5, 150 mM NaCl, and 1 mM cystine (Alfa Asar). The SEC buffer contained 20 mM HEPES pH8.5, 150 mM NaCl, 1 mM Cystine, and 0.06% Digitonin. To assemble cystinosin-Fab[3H5] complex, purified cystinosin was incubated with Fab[3H5] at a 1:1.5 molar ratio at 4 °C for 30 minutes. The mixture was then purified by SEC using the aforementioned buffers (Figure S3G). Peak fractions were collected and concentrated to ~5 mg/ml for grid preparation.

Generation of anti-human cystinosin antibody 3H5—IgG-3H5, a mouse monoclonal anti-human cystinosin antibody, was prepared by fusion of SP2-mIL6 mouse myeloma cells (ATCC no. CRL-2016) with splenic B lymphocytes obtained from BALB/c mice (n = 2) at UT Southwestern with the approval of the Institutional Animal Care and Research Advisory Committee #2017-102391 as previously described (Sun et al., 2021). Briefly, mice were immunized with one primary and eight boosts of purified recombinant human cystinosin reconstituted in amphipols (50 μg) in phosphate buffered saline (PBS) combined with Sigma Adjuvant System. Hybridomas were initially grown in HAT (hypoxanthine-aminopterin-thymidine) medium (DMEM high glucose supplemented with 20% FBS, 10% NCTC 109, and 1% each of HAT, ITS, NEAA, NaPyr, GlutaMAX, and Pen/strep). Hybridoma culture supernatants were screened by ELISA and counter-screened by western blot to select ELISA positive, western blot negative clones. One such hybridoma, designated IgG-3H5 (subclass IgG1), was subcloned by serial dilution three times and grown up in roller bottles in HT medium (DMEM high glucose supplemented with 10% FBS, 10% NCTC 109, and 1% each of HT, ITS, NEAA, NaPyr, GlutaMAX, and Pen/strep). IgG-3H5 was then purified from the hybridoma culture supernatant by gravity-flow affinity chromatography on protein G Sepharose 4 Fast Flow columns (Cytiva). The Fab fragment was generated by Papain cleavage in buffer containing 20 mM HEPES pH7.5, 150 mM NaCl, 10 mM cysteamine hydrochloride, 10 mM β-mercaptoethanol, and 10 mM EDTA. After incubation at 37 °C for 2 hours, the reaction was stopped by adding iodoacetamide to a final concentration of 23 mM and then incubated at room temperature for 20 minutes. The protein mixture was dialyzed overnight in buffer containing 10 mM HEPES pH7.5 and 10

mM NaCl. Fab[3H5] was further purified by a Hitrap Q column (Cytiva) and used for cryo-EM studies.

Nanobody selection and purification—Nanobody against human cystinosin was obtained through phage display following published protocols (McMahon et al., 2018; Pardon et al., 2014). Purified recombinant cystinosin with mutation of glycosylation sites (N36A, N41A, N51A, N66A, N84A, N104A and N107A) in the NTD was used to screen specific binders. After four rounds of selection, nanobody clones that bound to cystinosin were isolated and sequenced. Individual nanobody was expressed in *E.coli* BL21 (DE3) and purified by HisPur cobalt resin (ThermoScientific) according to the standard protocol (Pardon et al., 2014). Purified nanobodies were assessed by their ability of cystinosin binding through both pull-down assay and analytical SEC. Selenomethionine (Se-Met) labeled nanobody was expressed according to a standard protocol (Doublié, 1997). Nanobody P10 and Se-Met labeled P10 were purified similarly and used for co-crystallization with cystinosin.

Crystallization and crystal structure determination.—Cystinosin and nanobody P10 were incubated at a 1:1.5 molar ratio for 30 min and purified by SEC. Peak fractions containing cystinosin-P10 complex were concentrated to a final concentration of 60 mg/ml. Cystinosin-P10 complex was reconstituted into lipidic cubic phase (LCP) by mixing protein with monoolein (Sigma) at a 2:3 ratio (w/w) (Caffrey and Cherezov, 2009). Crystals were grown in 12% PEG400, 80 mM Li_2SO_4, and 50 mM MES pH 6.0 at 20 °C. Diffraction data were collected from multiple crystals, processed with HKL2000 (Otwinowski and Minor, 1997), and merged using XDS (Kabsch, 2010). The initial molecular replacement was carried out using truncated and modified nanobody Nb80 (Rasmussen et al., 2011) and truncated and modified EcSemiSWEET (Lee et al., 2015) as the search models in Phaser (McCoy et al., 2007). For the complex with Se-Met nanobody, selenium atoms of Se-Met nanobody were located by MR-SAD in Phaser. Model building and refinement cycles were carried out in Coot (Emsley and Cowtan, 2004) and Phenix (Adams et al., 2010). Structural figures were prepared using PyMOL (Schrödinger, LLC).

EM sample preparation and imaging for 300 kV Cryo-TEM—The cystinosin-Fab[3H5] complex samples (~5 mg/ml) were applied to Quantifoil R1.2/1.3 400 mesh Au holey carbon grids (Quantifoil). The grids were then blotted and plunged into liquid ethane for flash freezing using a Vitrobot Mark IV (FEI). The grids were imaged in a 300 kV Titan Krios (FEI) with a Gatan K3 Summit direct electron detector (Gatan). Data were collected using SerialEM (Mastronarde, 2005) at 0.842, 0.844, 0.83 Å/pixel. Images were recorded for 5 second exposures in 50 subframes with a total dose of ~60 electrons per $Å^2$.

Imaging processing and 3D reconstruction for 300kV Cryo-TEM—The images were collected in five sessions corresponding to the sample conditions and corresponding conformations of cystinosin: apo lumen-open conformation (5258 movies from 400 mesh grids, Figure S3A–C); apo cytosol-open conformation (7133 movies from 400 mesh grids, Figure S3D–F); cystine-bound lumen-open conformation (4991 movies from 400 mesh grids, Figure S3H–J); N288K at pH 5.0 (6642 movies from 400 mesh grids, Figure S7A–C);

N288K at pH 7.5 (3970 movies from 400 mesh grids, Figure S7D–F). Dark subtracted images were first normalized by gain reference. Motion correction was performed using the program MotionCor2 (Li et al., 2013). The contrast transfer function (CTF) was estimated using CTFFIND4 (Rohou and Grigorieff, 2015). Autopicking was performed with crYOLO v1.7.6 using a general model (Wagner et al., 2019), and a particle threshold of 0.2. About 0.7 – 1.5 million particles were extracted for each dataset. Subsequent 2D classification, multi-class Ab-Initio modeling, heterogenous 3D refinement, and non-uniform refinement of the best class were performed for all datasets in cryoSPARC v3.1.0 (Figures S3 and Figure S7). For the two apo conformations, further 3D classification, refinements with and without masks and Baysian polishing were performed in RELION-3.1 (Zivanov et al., 2018). The final maps for the apo conformations were then obtained with a final non-uniform refinement in cryoSPARC using the polished particles from RELION-3.1.

Cryo-EM model building and refinement—The initial model was built de novo and then manually adjusted using COOT (Emsley and Cowtan, 2004). Large aromatic/hydrophobic residues were assigned to facilitate the register of the transmembrane helices. In the cryo-EM structures, the densities of residues 1–24 of human cystinosin were neither resolved nor built. Residues 358–400 were also not built due to limited local resolution. The model was refined in real space using PHENIX (Adams et al., 2010). For cross-validations, the final model was refined against one of the half maps generated by 3D auto-refine and the model vs. map FSC curves were generated in the Comprehensive Validation module in PHENIX. PHENIX and MolProbity (Chen et al., 2010b) was used to validate the final model. Local resolutions were estimated using cyroSPARC local resolution estimation (Punjani et al., 2017). Structure Figures were generated using PyMOL (http://www.pymol.org) and Chimera (Pettersen et al., 2004).

Cystine uptake assay—The cystine transport activity was measured by an established cell-based uptake assay with minor modifications (Cherqui et al., 2001; Kalatzis et al., 2001). WT and mutants (residues 22–362) were cloned into a pEGFP-N1 vector with an N-terminal HA signal peptide followed by a Flag epitope. Plasmids were transfected into HEK-293S cells in 24-well plates using Lipofectamine 3000 (Invitrogen). After 24 hours, cells were washed twice with 500 μl buffer A (20 mM HEPES pH 7.5, 140 mM NaCl, 1 mM $MgSO_4$, 5 mM Glucose). Cystine uptake was performed at room temperature for 10 min, by incubating cells with 15 μM cold cystine and 0.5 μM [^{14}C]-cystine (200 mCi/mmol, PerkinElmer) in 200 μl buffer B (20 mM MES pH 5.2, 140 mM NaCl, 1 mM $MgSO_4$, 5 mM Glucose). The reaction was stopped by two washes with ice-cold buffer A. Cells were lysed with 1% sodium dodecyl sulfate (SDS) and subjected to scintillation counting. The concentration-dependent cystine uptake was carried out by a similar procedure, with different concentrations of cold cystine supplemented in buffer B. The uptake activities of cystinosin mutants were normalized to the level of protein expressed on the plasma membrane (except G337R and L338P, which cause protein destabilization/misfolding and show no detectable surface expression). Cell-surface expression of cystinosin mutants was assessed by anti-FLAG M1 antibody staining. At 24 hours post transfection, cells were washed twice with staining buffer (buffer A supplemented with 2mM $CaCl_2$), then incubated with anti-FLAG M1 antibody labeled with Alexa647 (Alexa Fluor647 NHS Ester,

Invitrogen) for 30 min at 4 °C. To saturate cystinosin molecules on cell surface, 2.0×10^5 cells were stained with M1-647 antibody at a final concentration of 1 μM. After another two washes with ice-cold staining buffer, cells were analyzed by BD Accuri C6 Plus flow cytometer. Experiments were repeated three times and surface-expression levels of cystinosin variants were quantified by the mean fluorescence of Alexa647 (Figure S4H). To assess the biochemical behavior of cystinosin mutants, cells were solubilized for 1 hour at 4 °C in solution containing 20 mM HEPES pH7.4, 150 mM NaCl, 1% DDM and 0.1% CHS. The clarified lysate was analyzed by fluorescence-detection size-exclusion chromatography (FSEC) and cystinosin-EGFP was monitored using excitation wavelength of 487 nm and emission wavelength of 507 nm (Figure S4J).

Generation of the stable cell lines—Stable cell lines were generated using lentiviruses following a previously established protocol (Andrzejewska et al., 2016). Briefly, human cystinosin-GFP and its related mutants including N288K, D205N, D305N, D346N were cloned into a lentiviral vector pLVX-EF1a-IRES-Puro. 5 mg of cystinosin plasmid was co-transfected with 2 mg pMD2G and 3 mg pSPAX2 (packaging plasmids) into HEK293T cells using X-tremeGENE HP DNA transfection reagent. After 24 hours, cell medium was changed from high glucose DMEM (Gibco) with 10% FCS, 1% L-glutamine and 1% Penicillin-Streptomycin to high glucose DMEM (Gibco) supplemented with 30% FCS, 1% L-glutamine and 1% Penicillin-Streptomycin at 37 °C with 5% CO_2. The supernatant was collected at 48 hours and 72 hours, and filtered through 0.45-mM pore size filters, yielding 7X lentiviral particles that were ready for use. NIH/3T3 cells were maintained in high glucose DMEM (Gibco) with 10% newborn calf serum and 1% Penicillin-Streptomycin at 37 °C with 8.8% CO_2. To establish NIH/3T3 stable cell lines, cells were infected with 1X lentiviral supernatant in the presence of polybrene (final concentration of 8 mg/ml). At 48 hours post-infection, cells were selected by adding puromycin to a final concentration of 1μg/ml for 2 weeks before the Co-IP assay.

Co-IP and Western Blotting—Co-immunoprecipitation (Co-IP) assay was performed as described previously (Andrzejewska et al., 2016). NIH/3T3 cells with stably expressed cystinosin WT and mutants were collected using a cell scraper, rinsed by PBS and lysed in cold lysis buffer (50 mM Tris, 150 mM NaCl, 1% Triton X-100, EDTA-free protease inhibitor (Roche), pH 7.5) for 30 mins. After centrifugation at 1000 g for 10 min, the supernatants were quantified by a bicinchoninic acid assay. Commercial μMACS GFP Microbeads Isolation Kit (Miltenyi Biotec) was used to perform the co-IP assay. According to the manufacturer's recommendation, 50 μl μMACS Anti-GFP microbeads were mixed with 2 mg of the input proteins for 1 hour on ice. The mixture was then applied to the μMACS separation columns equilibrated with lysis buffer, washed and eluted with the kit buffers. The immunoprecipitated proteins were resolved by SDS-PAGE and analyzed by Western blotting with antibodies against RagA (Cell Signaling Technology, 4357S), RagC (Cell Signaling Technology, 3360S), p18 (Cell Signaling Technology, 8975S), ATP6V1A (Santa Cruz Biotechnology, sc-293336), and GFP (Invitrogen, MA5-15256-HRP). Experiments were repeated three times. Similar results were obtained.

DEER sample preparation—DEER sample preparation utilized a cysteine-free version of human cystinosin (22–362) with mutations C223A, C224A, C268A, and C355A. Sites of interest were mutated to cysteine for site-specific spin labeling: S203C and Y321C were selected to probe the luminal ends, and two endogenous cysteine residues C224 and C355 were employed as the cytosolic label positions. DEER constructs were expressed and purified as described in the protein expression and purification section. 10 mM dithiothreitol was added to protein eluate from the cobalt column and removed by SEC right before spin labeling. Purified protein was incubated with a 40-fold molar excess of 1-oxyl-2,2,5,5-tetramethylpyrroline-3-methyl-methanethiosulfonate (MTSSL, Enzo LifeScience). The labeling reaction was performed at 4 °C overnight, followed by SEC to remove unreacted MTSSL. Labeled samples were buffer exchanged into desired pH values by diafiltration using a 50 kDa concentrator. Samples were concentrated to 100–150 μM and were measured by continuous wave EPR to verify a labelling efficiency of 60% or higher. The samples were then prepared at 20 μM with 30% deuterated glycerol for DEER experiments.

Reconstitution of cystinosin—Lipids consisting of 1:1:1 DOPC: DOPG: DOPE were dried under argon gas and washed twice in pentane to remove chloroform. To make preformed liposomes, lipids were resuspended at 20 mg/ml in Buffer 7.4 (10mM HEPES and 150mM NaCl at pH 7.4) or Buffer 5.2 (10mM MES and 150mM NaCl at pH 5.2), and frozen and thawed ten times in liquid nitrogen. For reconstitution, liposomes were extruded through 0.4 μm membrane filters and incubated with 1% n-octyl-β-d-glucoside (β-OG; Anatrace) for 1 hour at 4°C. Spin-labeled cystinosin was added into liposome/β-OG mixture at a protein: lipid ratio of 1: 33 (w/w) and incubated for 2 hours at 4°C. β-OG was removed by adding 250mg/ml biobeads (BioRad) in four batches over 18 hours. The proteoliposomes were homogenized by another ten freeze-and-thaw cycles and extrusion through 0.4 μm membrane filters, and then harvested by ultracentrifugation at 60,000 g for 1 hour. To prepare samples with a proton gradient (Figure S6F), proteoliposomes carrying spin labeled cystinosin at S203C/Y321C were prepared in Buffer 5.2 and treated with TCEP at a cystinosin:TCEP molar ratio of 1:50. 100 mM TCEP solution was made in Buffer 5.2. The removal of exterior spin labels was monitored by EPR (Figure S6G–H). After 6 hours, the exterior buffer of proteoliposomes was adjusted to pH 7.4 with 1M HEPES pH7.4. Samples were flash frozen at a protein concentration of 40 μM with 10% deuterated glycerol for DEER experiments.

Deglycosylation assay—Cystinosin is heavily glycosylated in the NTD. To determine the orientation of reconstituted cystinosin, 10–20 μg protein in liposomes were incubated with 50 units Endo D (NEB) at 37 °C for 3 hours. The reaction was stop by $4 \times$ SDS-loading buffer and protein was analyzed by SDS-PAGE gel (Figure S6D).

ACMA assay—The assay was adapted from fluorescence-based ion flux assay (Feng et al., 2012) (Figure S6B–C). In brief, 2 μl of 100 μM cystinosin in pH 5.2 liposomes was added into 150 μl Buffer 7.4 in the presence of 2 μM 9-amino-6-chloro-2-methox-yacridine (ACMA). The fluorescence (excitation:410nm; emission: 490nm) was monitored every second. Once the fluorescence signal stabilized, 1μM proton ionophore carbonyl cyanide

m-chlorophenyl hydrazone (CCCP) was added. The proton gradient was collapsed with the addition of 2 μM monensin. Proteoliposomes that have been treated with TCEP were washed twice before applying to ACMA assay. Experiments were repeated three times.

DTNB assay—20 mg/ml liposomes were loaded with 500 μM 5,5′-Dithiobis (2-nitrobenzoic acid) (DTNB) by ten freeze-and-thaw cycles in liquid nitrogen. DTNB-loaded liposomes were extruded through 0.4 μm membrane filters and washed twice with Buffer 7.4 to remove exterior DTNB. The reduction of DTNB resulted in an increase of absorbance at 412 nm. To assess the membrane permeability of TCEP, 2 mg/ml DTNB-loaded liposomes were monitored at 412 nm every 30 seconds for 6 hours in the presence of 1 mM TCEP. β-OG solubilized liposomes were recorded to measure maximum signal of reduced DTNB (Figure S6E). Experiments were repeated three times.

Substituted single-cysteine accessibility assay (SCAM)—Two cysteine reporters, Y281C and S312C, were introduced into the cysteine-free version of human cystinosin (residues 22–362) separately. WT-like cystinosin and its mutants including N288K, D205N, D305N, D346N were cloned into the pEGFP-N1 vector with an N-terminal HA signal peptide and a C-terminal GFP-His tag. Plasmids were transfected into HEK-293S cells in 6-well plates using Lipofectamine 3000 (Invitrogen). After 48 hours, cells were washed twice with 1 ml Buffer A (20 mM HEPES pH 7.5, 140 mM NaCl, 1 mM MgSO$_4$, 5 mM Glucose) and incubated with the membrane permeable thiol-reagent N-ethylmaleimide (NEM) at a concentration of 1 mM at 37 °C for 1 hour. The reaction was stopped by adding 10 mM cysteine. Cells were washed twice with PBS and then solubilized for 1 hour at 4 °C in solution containing 20 mM HEPES pH7.0, 150 mM NaCl, 1% DDM and 0.1% CHS. The clarified lysate was affinity purified by HisPur cobalt resin. Cystinosin-GFP eluate was treated with 1 mM 5K-PEG maleimide at 37 °C for 1 hour in the presence of 0.2% SDS, and 10 mM DTT was added to stop the reaction. Modified cystinosin-GFP was detected by SDS-PAGE using in-gel fluorescence. Experiments were repeated three times. Band intensities (I) were quantified by ImageJ. The modification efficiency of NEM was determined by $I_{\text{lower-band}} / [I_{\text{lower-band}} + I_{\text{upper-band}}]$.

EPR measurements—4-pulse DEER data was collected on a Bruker ELEXSYS E580 AWG spectrometer at Q Band equipped with a QT2 resonator. The pump pulse was fixed to the center peak in the field swept nitroxide spectrum and the probe frequency was chosen 100 MHz away from this frequency. π/2 and π pulses were all 44–54 ns gaussian pulses (Teucher and Bordignon, 2018) depending on the available power at time of measurement. The delay between the first and second probe pulses was 400 ns and dipolar evolution data was collected out to 2.5–3.5 μs. Experiments were run at 50 K and were signal averaged for 4–16 hrs. The raw data was background corrected and analyzed by Tikhonov regularization using DEERAnalysis2019 (Jeschke et al., 2006). CW-EPR spectra of the DEER samples were recorded at room temperature with a Bruker E500 CW-EPR spectrometer operating at the X-band frequency (~9.4 GHz) using an ER 4122SHQE resonator (Bruker).

Simulations of the DEER data were performed with MMM 2018 (2018 version available at https://epr.ethz.ch/software/older-versions/old_mmm.html) (Polyhach et al., 2011). Pre-calculated spin label rotamers were modeled into the labeling site on the static protein.

High energy states resulting from steric clashes with the protein backbone or side chains are excluded. Consequently, only low energy states compatible with the spin label attached to the static protein structure in the lumen-open or cytosol-open are retained. The collections of these static states represent the theoretical distribution of side chain conformers resolvable by EPR DEER measurements.

QUANTIFICATION AND STATISTICAL ANALYSIS

Statistical analyses of cystine uptake were performed using Prism6 (GraphPad Software Inc.). Saturation transport data in Figure 4D were fit into a Michaelis-Menten model. Data are expressed as mean ± s.e.m calculated in at least three independent experiments. Surface expression of cystinosin was quantified by mean fluorescence of Alexa647 of live single cell events via standard SSC/FSC gating using BD Accuri C6 Plus software.

Supplementary Material

Refer to Web version on PubMed Central for supplementary material.

ACKNOWLEDGEMENTS

REFERENCES

Abu-Remaileh M, Wyant GA, Kim C, Laqtom NN, Abbasi M, Chan SH, Freinkman E, and Sabatini DM (2017). Lysosomal metabolomics reveals V-ATPase- and mTOR-dependent regulation of amino acid efflux from lysosomes. Science 358, 807–813. [PubMed: 29074583]

Adams PD, Afonine PV, Bunkóczi G, Chen VB, Davis IW, Echols N, Headd JJ, Hung LW, Kapral GJ, Grosse-Kunstleve RW, et al. (2010). PHENIX: a comprehensive Python-based system for macromolecular structure solution. Acta Crystallogr. D 66, 213–221. [PubMed: 20124702]

Amick J, Tharkeshwar AK, Talaia G, and Ferguson SM (2020). PQLC2 recruits the C9orf72 complex to lysosomes in response to cationic amino acid starvation. J. Cell Biol 219.

Andrzejewska Z, Nevo N, Thomas L, Chhuon C, Bailleux A, Chauvet V, Courtoy PJ, Chol M, Guerrera IC, and Antignac C (2016). Cystinosin is a Component of the Vacuolar H+-ATPase-Ragulator-Rag Complex Controlling Mammalian Target of Rapamycin Complex 1 Signaling. J. Am. Soc. Nephrol 27, 1678–1688. [PubMed: 26449607]

Bissa B, Beedle AM, and Govindarajan R (2016). Lysosomal solute carrier transporters gain momentum in research. Clin. Pharmacol. Ther 100, 431–436. 10.1002/cpt.450. [PubMed: 27530302]

Bräuer P, Parker JL, Gerondopoulos A, Zimmermann I, Seeger MA, Barr FA, and Newstead S (2019). Structural basis for pH-dependent retrieval of ER proteins from the Golgi by the KDEL receptor. Science 363, 1103–1107. [PubMed: 30846601]

Bröer S, and Bröer A (2017). Amino acid homeostasis and signalling in mammalian cells and organisms. Biochem. J 474, 1935–1963. [PubMed: 28546457]

Bulut H, Moniot S, Licht A, Scheffel F, Gathmann S, Saenger W, and Schneider E (2012). Crystal structures of two solute receptors for L-cystine and L-cysteine, respectively, of the human pathogen Neisseria gonorrhoeae. J. Mol. Biol 415, 560–572. [PubMed: 22138345]

Caffrey M, and Cherezov V (2009). Crystallizing membrane proteins using lipidic mesophases. Nat. Protoc 4, 706–731. [PubMed: 19390528]

Chen LQ, Hou BH, Lalonde S, Takanaga H, Hartung ML, Qu XQ, Guo WJ, Kim JG, Underwood W, Chaudhuri B, et al. (2010a). Sugar transporters for intercellular exchange and nutrition of pathogens. Nature 468, 527–532. [PubMed: 21107422]

Chen VB, Arendall WB, Headd JJ, Keedy DA, Immormino RM, Kapral GJ, Murray LW, Richardson JS, and Richardson DC (2010b). MolProbity: all-atom structure validation for macromolecular crystallography. Acta Crystallogr. D 66, 12–21. [PubMed: 20057044]

Cherqui S, and Courtoy PJ (2017). The renal Fanconi syndrome in cystinosis: pathogenic insights and therapeutic perspectives. Nat. Rev. Nephrol 13, 115–131. [PubMed: 27990015]

Cherqui S, Kalatzis V, Trugnan G, and Antignac C (2001). The targeting of cystinosin to the lysosomal membrane requires a tyrosine-based signal and a novel sorting motif. J. Biol. Chem 276, 13314–13321. [PubMed: 11150305]

Cline DJ, Redding SE, Brohawn SG, Psathas JN, Schneider JP, and Thorpe C (2004). New water-soluble phosphines as reductants of peptide and protein disulfide bonds: reactivity and membrane permeability. Biochemistry 43, 15195–15203. [PubMed: 15568811]

David D, Princiero Berlingerio S, Elmonem MA, Oliveira Arcolino F, Soliman N, van den Heuvel B, Gijsbers R, and Levtchenko E (2019). Molecular Basis of Cystinosis: Geographic Distribution, Functional Consequences of Mutations in the CTNS Gene, and Potential for Repair. Nephron 141, 133–146. [PubMed: 30554218]

Deutschmann S, Rimle L, and von Ballmoos C (2022). Rapid Estimation of Membrane Protein Orientation in Liposomes. Chembiochem 23, e202100543. [PubMed: 34763366]

Doublié S (1997). Preparation of selenomethionyl proteins for phase determination. Methods Enzymol. 276, 523–530.

Emsley P, and Cowtan K (2004). Coot: model-building tools for molecular graphics. Acta Crystallogr. D 60, 2126–2132. [PubMed: 15572765]

Feng L, Campbell EB, and MacKinnon R (2012). Molecular mechanism of proton transport in CLC Cl-/H+ exchange transporters. Proc. Natl Acad. Sci. USA 109, 11699–11704. [PubMed: 22753511]

Feng L, and Frommer WB (2015). Structure and function of SemiSWEET and SWEET sugar transporters. Trends Biochem. Sci 40, 480–486. [PubMed: 26071195]

Feng L, and Frommer WB (2016). Evolution of Transporters: The Relationship of SWEETs, PQ-loop, and PnuC Transporters. Trends Biochem. Sci 41, 118–119. [PubMed: 26749089]

Gahl WA (1987). Disorders of lysosomal membrane transport—cystinosis and Salla disease. Enzyme 38, 154–160. [PubMed: 3326729]

Gahl WA, Bashan N, Tietze F, Bernardini I, and Schulman JD (1982). Cystine transport is defective in isolated leukocyte lysosomes from patients with cystinosis. Science 217, 1263–1265. [PubMed: 7112129]

Gahl WA, Thoene JG, and Schneider JA (2002). Cystinosis. N. Engl. J. Med 347, 111–121. [PubMed: 12110740]

Goehring A, Lee CH, Wang KH, Michel JC, Claxton DP, Baconguis I, Althoff T, Fischer S, Garcia KC, and Gouaux E (2014). Screening and large-scale expression of membrane proteins in mammalian cells for structural studies. Nat. Protoc 9, 2574–2585. [PubMed: 25299155]

Han L, Zhu Y, Liu M, Zhou Y, Lu G, Lan L, Wang X, Zhao Y, and Zhang XC (2017). Molecular mechanism of substrate recognition and transport by the AtSWEET13 sugar transporter. Proc. Natl Acad. Sci. USA 114, 10089–10094. [PubMed: 28878024]

Jeschke G, Chechik V, Ionita P, Godt A, Zimmermann H, Banham J, Timmel CR, Hilger D, and Jung H (2006). DeerAnalysis2006—a comprehensive software package for analyzing pulsed ELDOR data. Appl. Magn. Reson 30, 473–498.

Jezegou A, Llinares E, Anne C, Kieffer-Jaquinod S, O'Regan S, Aupetit J, Chabli A, Sagne C, Debacker C, Chadefaux-Vekemans B, et al. (2012). Heptahelical protein PQLC2 is a lysosomal cationic amino acid exporter underlying the action of cysteamine in cystinosis therapy. Proc. Natl Acad. Sci. USA 109, E3434–3443. [PubMed: 23169667]

Jonas AJ, Smith ML, and Schneider JA (1982). ATP-dependent lysosomal cystine efflux is defective in cystinosis. J. Biol. Chem 257, 13185–13188. [PubMed: 6292178]

Jouandin P, Marelja Z, Shih Y-H, Parkhitko Andrey A, Dambowsky M, Asara John M, Nemazanyy I, Dibble Christian C, Simons M, and Perrimon N (2022). Lysosomal cystine mobilization shapes the response of TORC1 and tissue growth to fasting. Science 375, eabc4203. [PubMed: 35175796]

Kabsch W (2010). XDS. Acta Crystallogr. D 66, 125–132. [PubMed: 20124692]

Kalatzis V, Cherqui S, Antignac C, and Gasnier B (2001). Cystinosin, the protein defective in cystinosis, is a H(+)-driven lysosomal cystine transporter. EMBO J. 20, 5940–5949. [PubMed: 11689434]

Kalatzis V, Nevo N, Cherqui S, Gasnier B, and Antignac C (2004). Molecular pathogenesis of cystinosis: effect of CTNS mutations on the transport activity and subcellular localization of cystinosin. Hum. Mol. Genet 13, 1361–1371. [PubMed: 15128704]

Landau M, Mayrose I, Rosenberg Y, Glaser F, Martz E, Pupko T, and Ben-Tal N (2005). ConSurf 2005: the projection of evolutionary conservation scores of residues on protein structures. Nucleic Acids Res. 33, W299–302. [PubMed: 15980475]

Latorraca NR, Fastman NM, Venkatakrishnan AJ, Frommer WB, Dror RO, and Feng L (2017). Mechanism of Substrate Translocation in an Alternating Access Transporter. Cell 169, 96–107.e112. [PubMed: 28340354]

Lee Y, Nishizawa T, Yamashita K, Ishitani R, and Nureki O (2015). Structural basis for the facilitative diffusion mechanism by SemiSWEET transporter. Nat. Commun 6, 6112. [PubMed: 25598322]

Leray X, Conti R, Li Y, Debacker C, Castelli F, Fenaille F, Zdebik AA, Pusch M, and Gasnier B (2021). Arginine-selective modulation of the lysosomal transporter PQLC2 through a gate-tuning mechanism. Proc. Natl Acad. Sci. USA 118.

Li X, Mooney P, Zheng S, Booth CR, Braunfeld MB, Gubbens S, Agard DA, and Cheng Y (2013). Electron counting and beam-induced motion correction enable near-atomic-resolution single-particle cryo-EM. Nat. Methods 10, 584–590. [PubMed: 23644547]

Li X, Saha P, Li J, Blobel G, and Pfeffer SR (2016). Clues to the mechanism of cholesterol transfer from the structure of NPC1 middle lumenal domain bound to NPC2. Proc. Natl Acad. Sci. USA 113, 10079–10084. [PubMed: 27551080]

Liu B, Du H, Rutkowski R, Gartner A, and Wang X (2012). LAAT-1 is the lysosomal lysine/arginine transporter that maintains amino acid homeostasis. Science 337, 351–354. [PubMed: 22822152]

Lobry T, Miller R, Nevo N, Rocca CJ, Zhang J, Catz SD, Moore F, Thomas L, Pouly D, Bailleux A, et al. (2019). Interaction between galectin-3 and cystinosin uncovers a pathogenic role of inflammation in kidney involvement of cystinosis. Kidney Int. 96, 350–362. [PubMed: 30928021]

Lu M, Xu BY, Zhou K, Cheng W, Jiang YL, Chen Y, and Zhou CZ (2014). Structural and biochemical analyses of Microcystis aeruginosa O-acetylserine sulfhydrylases reveal a negative feedback regulation of cysteine biosynthesis. Biochim. Biophys. Acta 1844, 308–315. [PubMed: 24275508]

Mastronarde DN (2005). Automated electron microscope tomography using robust prediction of specimen movements. J. Struct. Biol 152, 36–51. [PubMed: 16182563]

McCoy AJ, Grosse-Kunstleve RW, Adams PD, Winn MD, Storoni LC, and Read RJ (2007). Phaser crystallographic software. J. Appl. Crystallogr 40, 658–674. [PubMed: 19461840]

McMahon C, Baier AS, Pascolutti R, Wegrecki M, Zheng S, Ong JX, Erlandson SC, Hilger D, Rasmussen SGF, Ring AM, et al. (2018). Yeast surface display platform for rapid discovery of conformationally selective nanobodies. Nat. Struct. Mol. Biol 25, 289–296. [PubMed: 29434346]

Nevo N, Thomas L, Chhuon C, Andrzejewska Z, Lipecka J, Guillonneau F, Bailleux A, Edelman A, Antignac C, and Guerrera IC (2017). Impact of Cystinosin Glycosylation on Protein Stability by Differential Dynamic Stable Isotope Labeling by Amino Acids in Cell Culture (SILAC). Mol. Cell Proteomics 16, 457–468. [PubMed: 28082515]

Otwinowski Z, and Minor W (1997). Processing of X-ray diffraction data collected in oscillation mode. Methods Enzymol. 276, 307–326. [PubMed: 27754618]

Pardon E, Laeremans T, Triest S, Rasmussen SG, Wohlkönig A, Ruf A, Muyldermans S, Hol WG, Kobilka BK, and Steyaert J (2014). A general protocol for the generation of Nanobodies for structural biology. Nat. Protoc 9, 674–693. [PubMed: 24577359]

Pettersen EF, Goddard TD, Huang CC, Couch GS, Greenblatt DM, Meng EC, and Ferrin TE (2004). UCSF Chimera—a visualization system for exploratory research and analysis. J. Comput. Chem 25, 1605–1612. [PubMed: 15264254]

Polyhach Y, Bordignon E, and Jeschke G (2011). Rotamer libraries of spin labelled cysteines for protein studies. Phys. Chem. Chem. Phys 13, 2356–2366. [PubMed: 21116569]

Punjani A, Rubinstein JL, Fleet DJ, and Brubaker MA (2017). cryoSPARC: algorithms for rapid unsupervised cryo-EM structure determination. Nat. Methods 14, 290–296. [PubMed: 28165473]

Rasmussen SG, Choi HJ, Fung JJ, Pardon E, Casarosa P, Chae PS, Devree BT, Rosenbaum DM, Thian FS, Kobilka TS, et al. (2011). Structure of a nanobody-stabilized active state of the β(2) adrenoceptor. Nature 469, 175–180. [PubMed: 21228869]

Rohou A, and Grigorieff N (2015). CTFFIND4: Fast and accurate defocus estimation from electron micrographs. J. Struct. Biol 192, 216–221. [PubMed: 26278980]

Ruivo R, Bellenchi GC, Chen X, Zifarelli G, Sagne C, Debacker C, Pusch M, Supplisson S, and Gasnier B (2012). Mechanism of proton/substrate coupling in the heptahelical lysosomal transporter cystinosin. Proc. Natl Acad. Sci. USA 109, E210–217. [PubMed: 22232659]

Saudek V (2012). Cystinosin, MPDU1, SWEETs and KDELR belong to a well-defined protein family with putative function of cargo receptors involved in vesicle trafficking. PLoS ONE 7, e30876. [PubMed: 22363504]

Schneider JA, Bradley K, and Seegmiller JE (1967). Increased cystine in leukocytes from individuals homozygous and heterozygous for cystinosis. Science 157, 1321–1322. [PubMed: 6038997]

Sun Y, Wang J, Long T, Qi X, Donnelly L, Elghobashi-Meinhardt N, Esparza L, Cohen JC, Xie XS, Hobbs HH, and Li X (2021). Molecular basis of cholesterol efflux via ABCG subfamily transporters. Proc. Natl Acad. Sci. USA 118, e2110483118. [PubMed: 34404721]

Talaia G, Amick J, and Ferguson SM (2021). Receptor-like role for PQLC2 amino acid transporter in the lysosomal sensing of cationic amino acids. Proc. Natl Acad. Sci. USA 118, e2014941118. [PubMed: 33597295]

Tao Y, Cheung LS, Li S, Eom JS, Chen LQ, Xu Y, Perry K, Frommer WB, and Feng L (2015). Structure of a eukaryotic SWEET transporter in a homotrimeric complex. Nature 527, 259–263. [PubMed: 26479032]

Teucher M, and Bordignon E (2018). Improved signal fidelity in 4-pulse DEER with Gaussian pulses. J. Magn. Reson 296, 103–111. [PubMed: 30241017]

Town M, Jean G, Cherqui S, Attard M, Forestier L, Whitmore SA, Callen DF, Gribouval O, Broyer M, Bates GP, et al. (1998). A novel gene encoding an integral membrane protein is mutated in nephropathic cystinosis. Nat. Genet 18, 319–324. [PubMed: 9537412]

Wagner T, Merino F, Stabrin M, Moriya T, Antoni C, Apelbaum A, Hagel P, Sitsel O, Raisch T, Prumbaum D, et al. (2019). SPHIRE-crYOLO is a fast and accurate fully automated particle picker for cryo-EM. Commun. Biol 2, 218. [PubMed: 31240256]

Wang J, Yan C, Li Y, Hirata K, Yamamoto M, Yan N, and Hu Q (2014). Crystal structure of a bacterial homologue of SWEET transporters. Cell Res. 24, 1486–1489. [PubMed: 25378180]

Wyant GA, Abu-Remaileh M, Wolfson RL, Chen WW, Freinkman E, Danai LV, Vander Heiden MG, and Sabatini DM (2017). mTORC1 Activator SLC38A9 Is Required to Efflux Essential Amino Acids from Lysosomes and Use Protein as a Nutrient. Cell 171, 642–654.e612. [PubMed: 29053970]

Xu Y, Tao Y, Cheung LS, Fan C, Chen L-Q, Xu S, Perry K, Frommer WB, and Feng L (2014). Structures of bacterial homologues of SWEET transporters in two distinct conformations. Nature 515, 448–452. [PubMed: 25186729]

Zhang J, Johnson JL, He J, Napolitano G, Ramadass M, Rocca C, Kiosses WB, Bucci C, Xin Q, Gavathiotis E, et al. (2017). Cystinosin, the small GTPase Rab11, and the Rab7 effector RILP regulate intracellular trafficking of the chaperone-mediated autophagy receptor LAMP2A. J. Biol. Chem 292, 10328–10346. [PubMed: 28465352]

Zivanov J, Nakane T, Forsberg BO, Kimanius D, Hagen WJ, Lindahl E, and Scheres SH (2018). New tools for automated high-resolution cryo-EM structure determination in RELION-3. Elife 7.

Highlights:

- Structures of human cystinosin are captured in cytosol-open and lumen-open states

- Cystine-bound structure and functional analyses demonstrate substrate selectivity

- DEER studies reveal proton-driven conformational changes

- Cystinosin engages the Ragulator-Rag components in a conformation-dependent manner
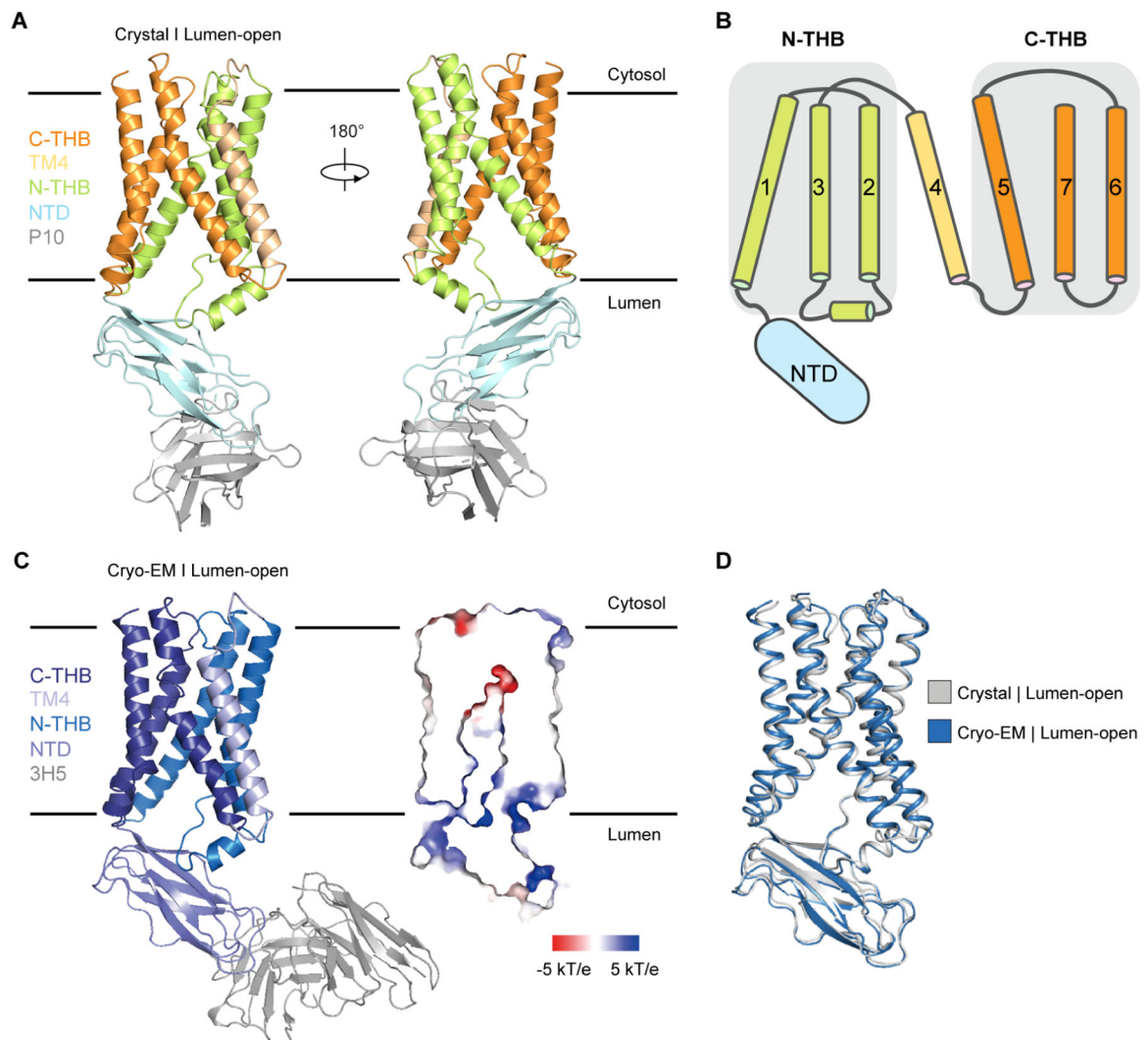
Figure 1. Structures of cystinosin in lumen-open conformation

(**A**) Crystal structure of cystinosin bound to nanobody P10. Colored by structural elements.

(**B**) Topology diagram of cystinosin.

(**C**) Cryo-EM structure of lumen-open cystinosin-Fab[3H5]. The ribbon representation (left) is colored by structural elements. The slab view (right) is colored by electrostatic potential (red, -5 kT e^{-1}; blue, $+5$ kT e^{-1}).

(**D**) Superposition of the lumen-open crystal (gray) and cryo-EM (blue) structures.

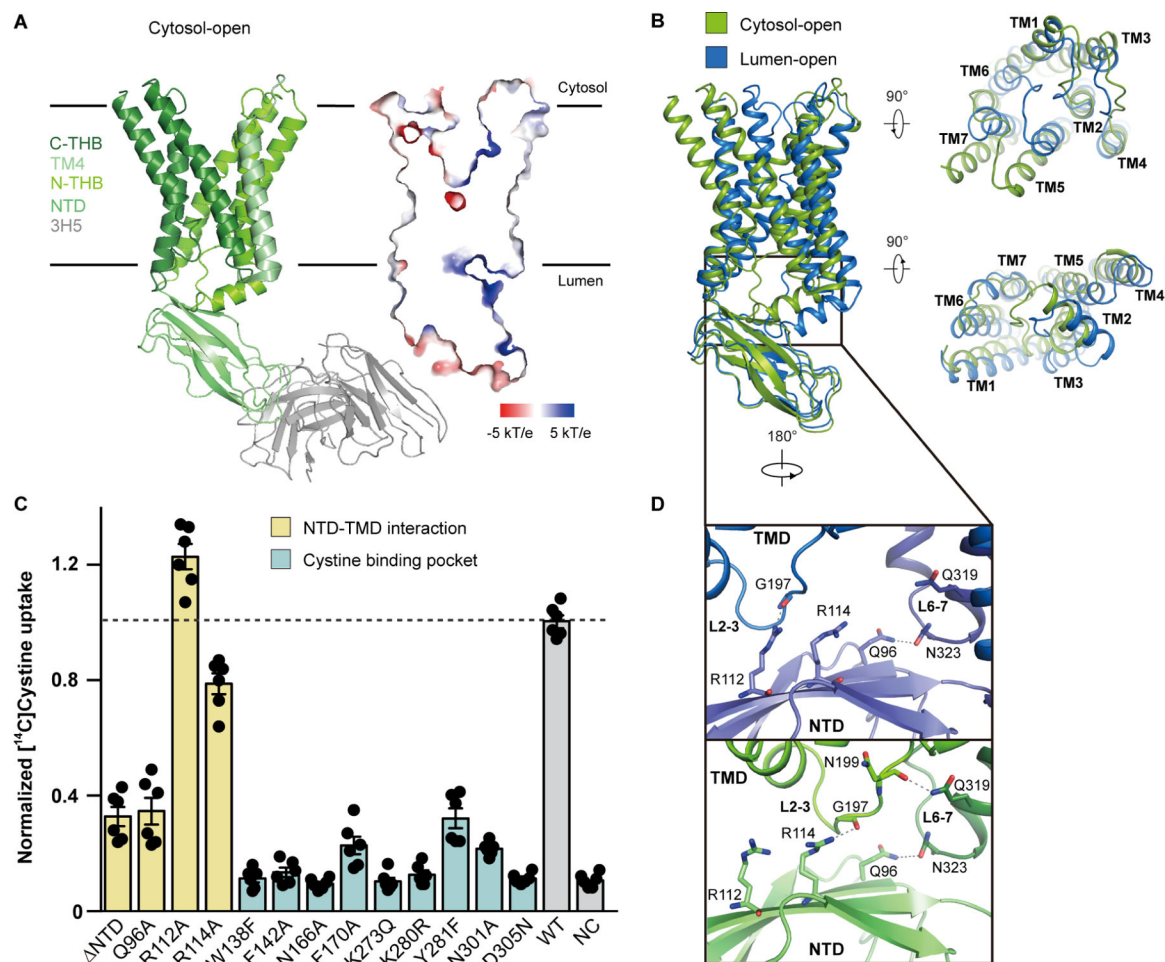See also Figures S2, S3, Tables S1 and S2.

Figure 2. Structure of cystinosin in the cytosol-open conformation

(A) Cryo-EM structure of cytosol-open cystinosin-Fab[3H5]. The ribbon representation (left) is colored by structural elements. The slab view (right) is colored by electrostatic potential (red, -5 kT e^{-1}; blue, $+5$ kT e^{-1}).

(B) Comparison of cytosol-open (green) and lumen-open (blue) cryo-EM structures. TM rearrangements are shown from the cytosol (top) and the lumen (bottom).

(C) Cystine uptake activities of cystinosin mutants, normalized to wild type (dashed line) (mean± s.e.m.; n=6 independent experiments). WT, wild type; NC, negative control.

(D) Close-up views of NTD-TMD interactions in lumen-open (blue) and cytosol-open (green) structures. Residues involved in NTD-TMD interactions are shown as sticks; gray dashes indicate hydrophilic interactions.

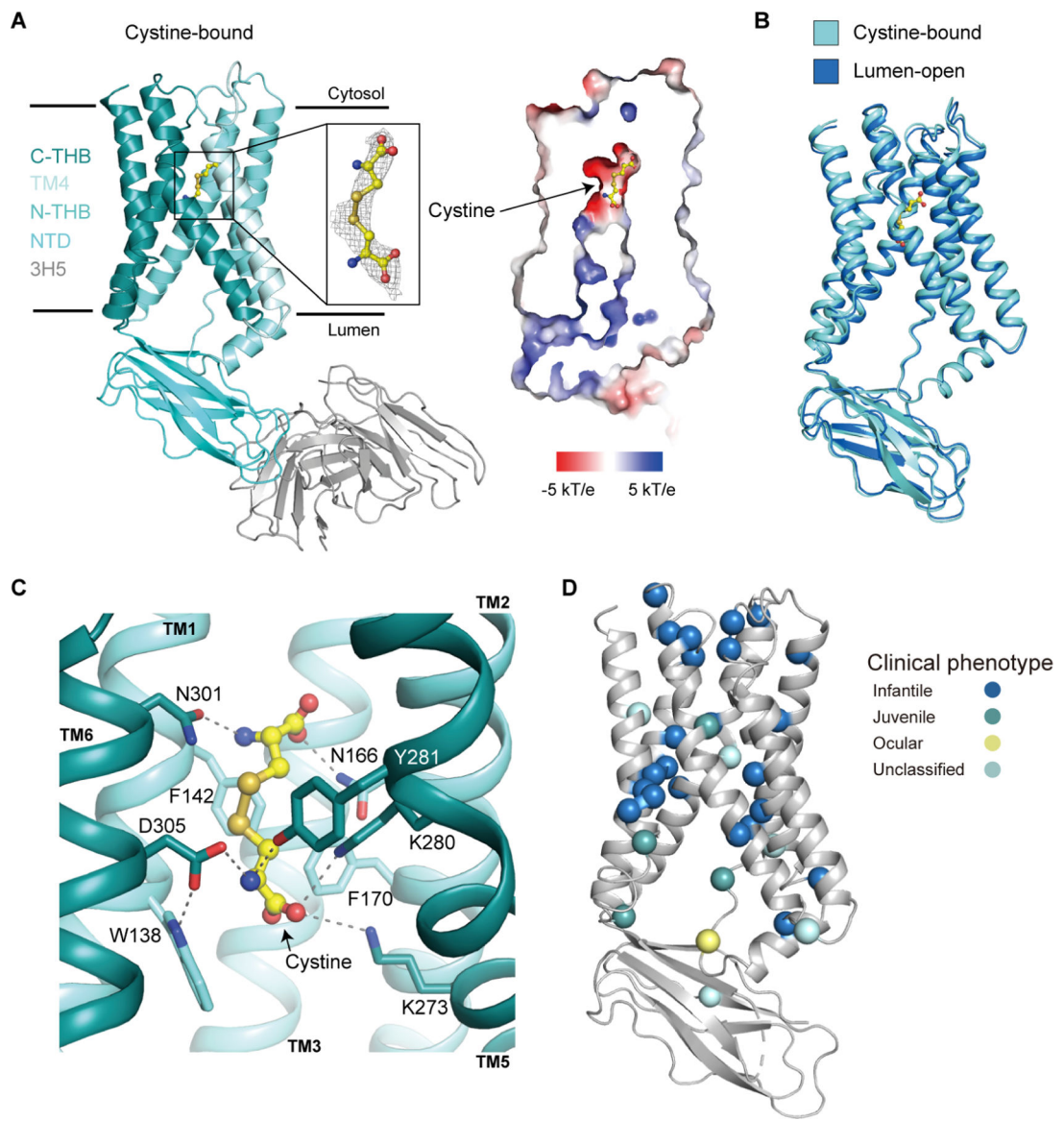See also Figures S3, S4 and Table S2.

Figure 3. Cystine binding and recognition

(A) Cryo-EM structure of cystine-bound cystinosin-Fab[3H5]. The ribbon representation (left) is colored by structural elements, with zoomed-in view of cystine density. The slab view (right) is colored by electrostatic potential (red, -5 kT e^{-1}; blue, $+5$ kT e^{-1}).

(B) Comparison of cryo-EM cystine-bound (cyan) and lumen-open (blue) structures.

(C) Cystine bound in the substrate binding pocket. Cystine-binding residues are shown as sticks; gray dashes indicate hydrophilic interactions.

(D) Cystinosis-associated missense mutations mapped onto the lumen-open structure. Mutations are shown as spheres and colored by clinical phenotypes, as indicated.

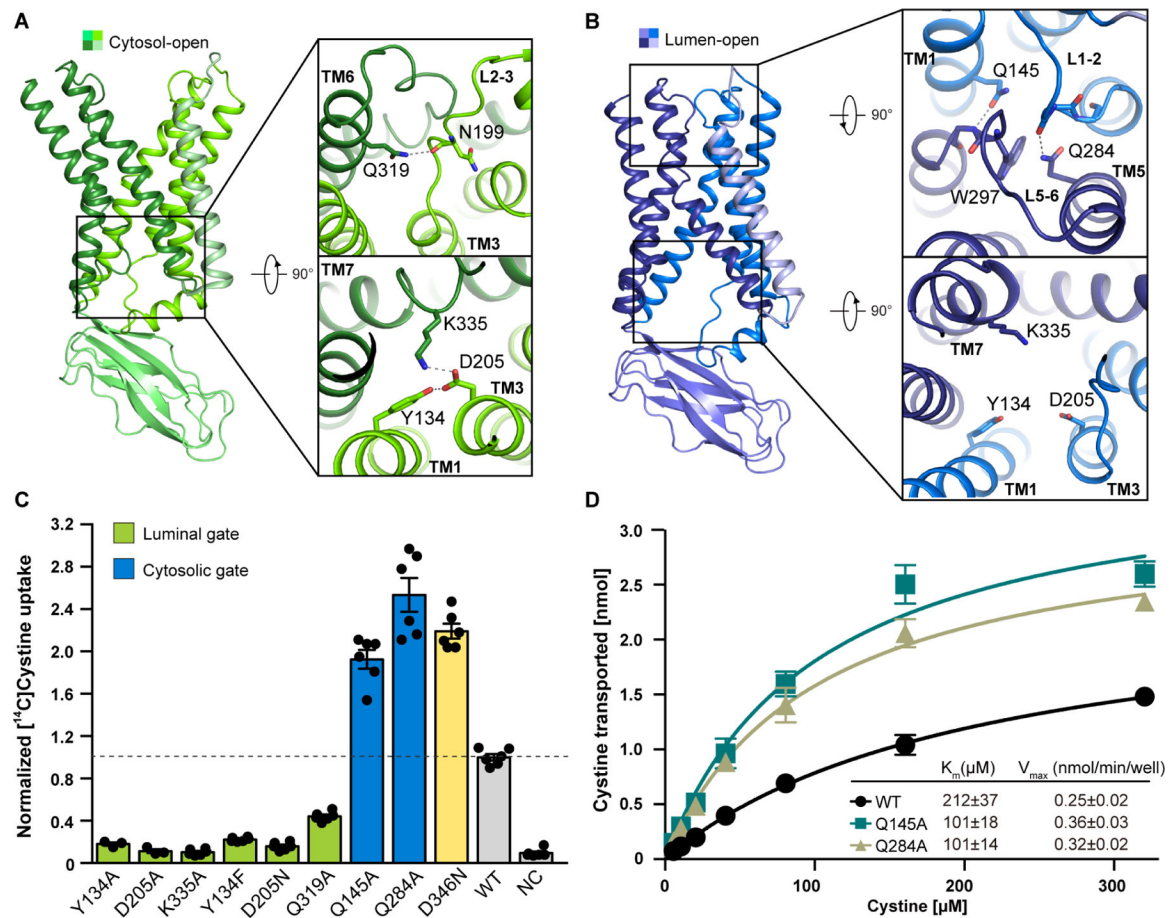See also Figures S3, S4 and Table S2.

Figure 4. Luminal and cytosolic gates of cystinosin

(A) Overall structure of cytosol-open cystinosin with close-up views of the luminal gate.

(B) Overall structure of lumen-open cystinosin with close-up views of cytosolic (top) and luminal (bottom) gates. The hydrophilic interactions in (A) and (B) are indicated by gray dashes. Residues involved in gate formation are shown as sticks.

(C) Cystine uptake activities of cystinosin with gate mutations or D346 mutation (yellow), normalized to WT (dashed line) (mean± s.e.m.; n= 3 or 6 independent experiments).

(D) Transport activities of WT, Q145A, and Q284A at various cystine concentrations (mean SEM; n = 3 independent experiments).
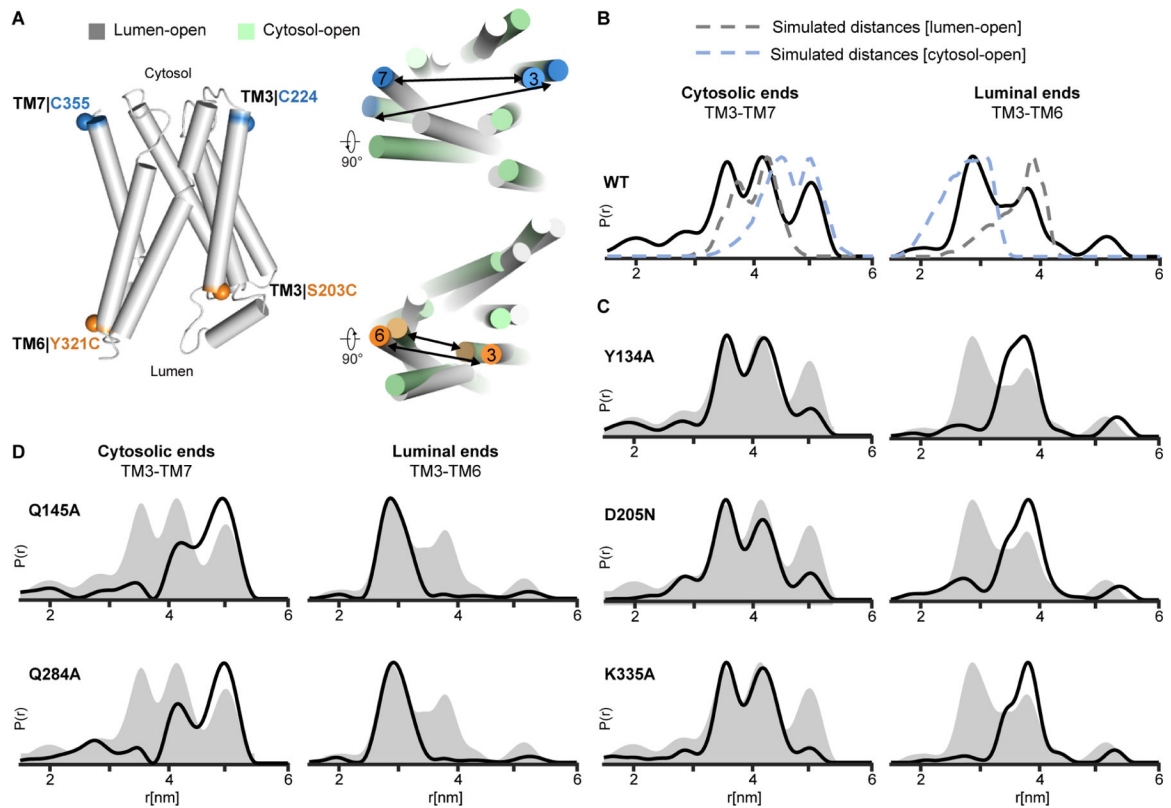
Figure 5. Conformational transitions of cystinosin

(**A**) Cartoon representation of the TMD with positions of spin label pairs highlighted in spheres.

(**B**) Distance distributions (solid line) between spin labels on cytosolic ends (left) and luminal ends (right). The dashed lines show simulated spin label distance distributions from lumen-open (gray) and cytosol-open (light blue) states. r indicates the interspin distance, and *P(r)* indicates the distance probability. DEER measurements were performed at pH7.4.

(**C**) Distance distributions of luminal gate mutants (solid line) on cytosolic ends (left) and luminal ends (right), with distances from WT overlaid as a gray shadow for comparison.

(**D**) Distance distributions of cytosolic gate mutants, shown as in (C).

See also Figure S5.
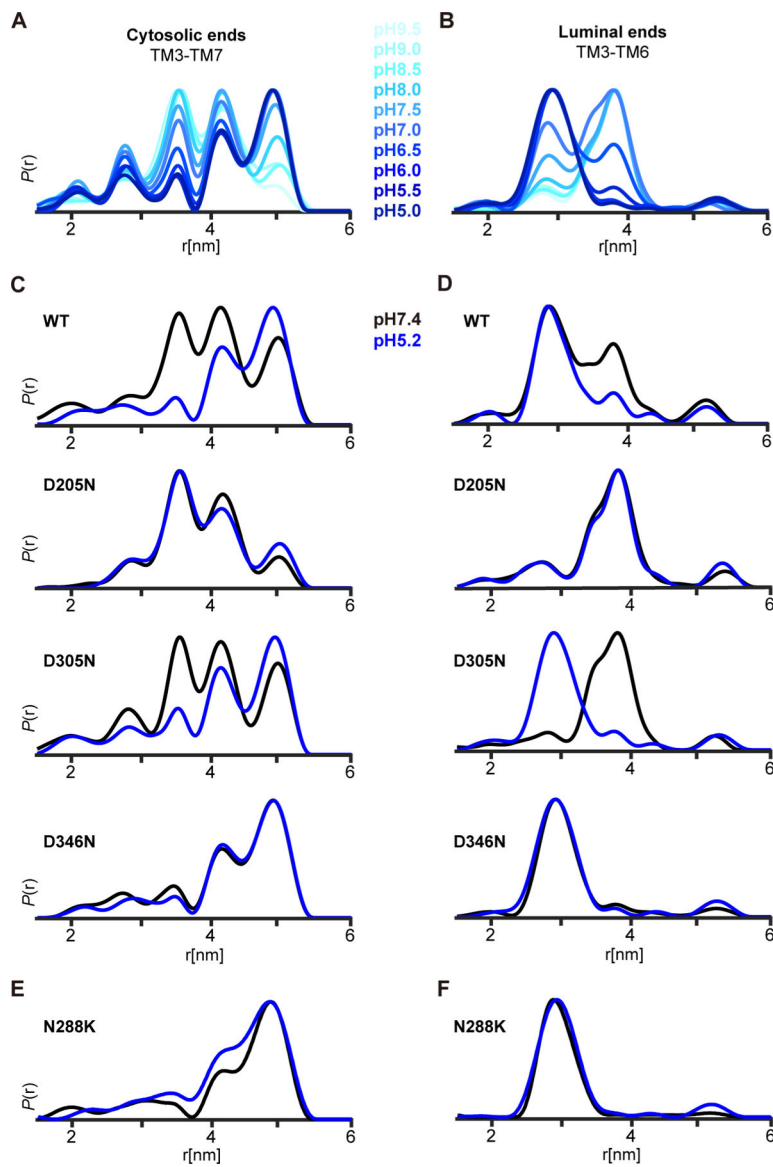
Figure 6. pH-dependent conformational changes of cystinosin

(A) and **(B)** Distance distributions of cytosolic ends (A) and luminal ends (B) obtained at 10 different pH values ranging from 9.5 to 5.0 (color gradient from cyan to blue).

(C) and **(D)** Distance distributions of protonation-mimicking mutants on cytosolic ends (C) and luminal ends (D) at pH7.4 (black) and pH5.2 (blue).

(E) and **(F)** Distance distributions of N288K on cytosolic ends (E) and luminal ends (F) at pH7.4 (black) and pH5.2 (blue).

See also Figures S5 and S6.
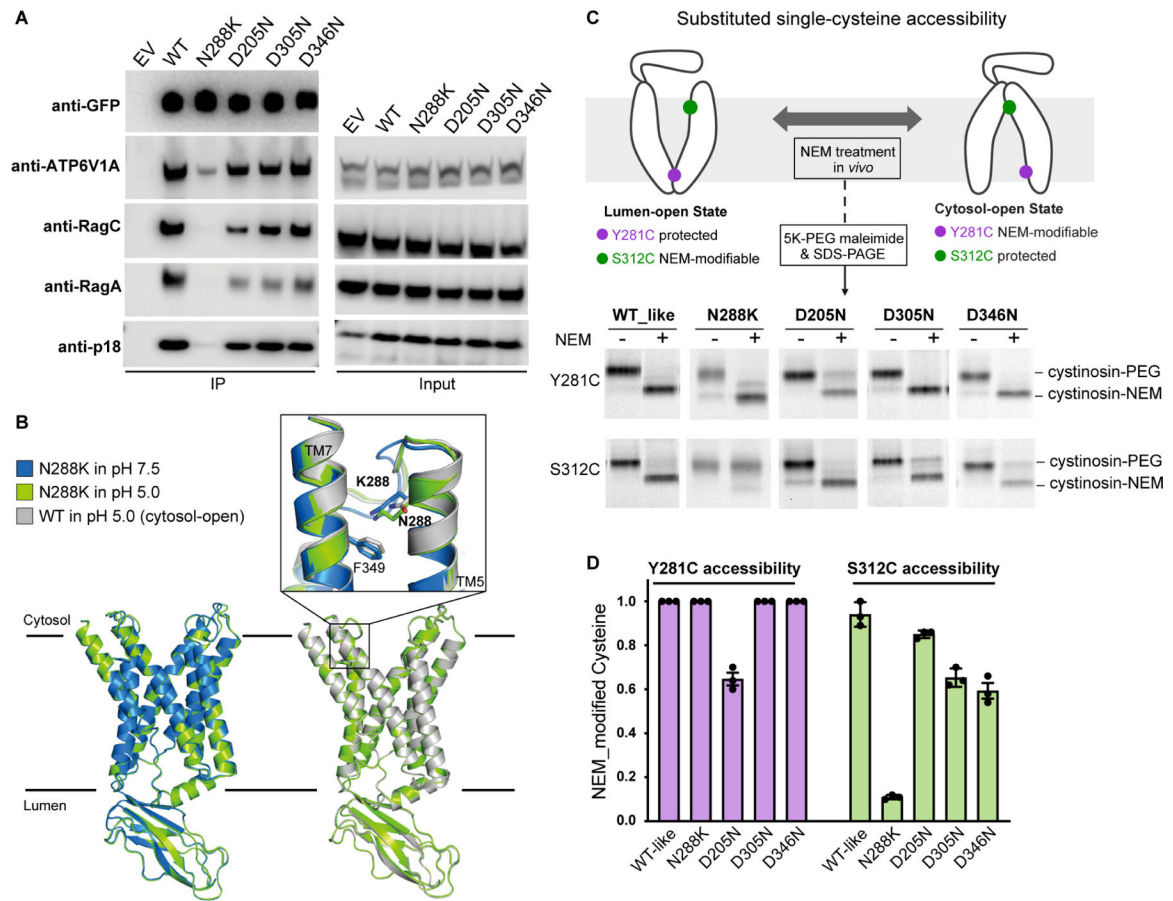
Figure 7. Cystinosin's conformational states and interaction with the Ragulator-Rag components
(A) Anti-GFP immunoprecipitation for the interaction between cystinosin-GFP and the Ragulator-Rag components. EV: empty vector.
(B) Overall structures of N288K variant in pH 7.5 and pH 5.0 (left), and comparison of the cytosol-open WT and N288K structures (right) with a close-up view of the N288K residue. **(C)** and **(D)** SCAM analysis of cystinosin WT and mutants. Two cysteine reporters were used to assess the conformational states: Y281C as a cytosol-open reporter; S312C as a lumen-open reporter. Experimental flowchart and SDS-PAGE of SCAM are shown in (C). NEM modification of Y281C and S312C are quantified in (D) (mean± s.e.m.; n=3 independent experiments).
See also Figure S7.

Key resources table

REAGENT or RESOURCE	SOURCE	IDENTIFIER
Antibodies		
Anti-FLAG M1	ATCC	Hybridoma HB-9259,RRID: CVCL_J730
Anti-FLAG M2	Sigma-Aldrich	F1804-59UG, RRID: AB_262044
Donkey Anti-mouse IgG, HRP conjugated	Jackson ImmunoResearch	715-035-150, RRID: AB_2340770
Goat Anti-mouse IgM, HRP conjugated	Jackson ImmunoResearch	115-035-075, RRID: AB_2338508
Monoclonal Anti-cystinosin 3H5	This paper	N/A
Anti-Rag A	Cell signaling Technology	4357S
Anti-Rag C	Cell signaling Technology	3360S
Anti-p18	Cell signaling Technology	8975S
Anti-ATP6V1A	Santa Cruz Biotechnology	Sc-293336
Anti-GFP	Invitrogen	MA5-15256-HRP
Chemicals, peptides, and recombinant proteins		
HisPur cobalt resin	Thermo Scientific	89966
Anti-Flag M2 resin	Millipore-Sigma	A2220
3X FLAG peptide	ApexBio	A6001
Protein G Sepharose 4 Fast Flow	Cytiva	17061805
Superdex 200 Increase 10/300 GL SEC column	Cytiva	28990944
R1.2/1.3 400 mesh Au holey carbon grids	Quantifoil	1210627
Monoolein	Sigma-Aldrich	M7765
Lauryl maltose neopentyl glycol (LMNG)	Anatrace	NG310
Cholesteryl hemisuccinate (CHS)	Anatrace	CH210
n-Dodecyl-b-D-Maltoside (DDM)	Anatrace	D310
Digitonin	ACROS Organics	407565000
n-octyl-β-d-glucoside	Anatrace	O311
DOPC	Avanti	850375
DOPG	Avanti	840475
DOPE	Avanti	850725
Phenylmethylsulfonyl fluoride (PMSF)	Goldbio	P-470-25
Leupeptin	Peptides International	ILP-4041
Papain	Worthington	LS003119
Cystine	Alfa Asar	AAA1376230
$[^{14}C]$-Cystine	PerkinElmer	NEC854
PEG 400	Affymetrix	19957
Lithium sulfate	Thermo Scientific	AC21832
Sodium butyrate	Thermo Scientific	A1107936
Alexa Fluor647 NHS Ester	Invitrogen	A20006
ACMA	Thermo Scientific	A1324
CCCP	Alfa Asar	L06932
Monensin	Millipore-Sigma	M5273
DTNB	Millipore-Sigma	D8130

REAGENT or RESOURCE	SOURCE	IDENTIFIER
TCEP	GoldBio	TCEP10
Endo D	NEB	P0742
N-Ethylmaleimide	Millipore-Sigma	04260
5K-PEG maleimide	Millipore-Sigma	63187
Lipofectamine 3000	Invitrogen	L3000001
ESF921 medium	Expression System	96-001
Sf-900 III SFM	Gibco	12658027
Freestyle™ 293 expression medium	Gibco	12338018
Fetal Bovine Serum	Corning	35015170
Medium NCTC-109 (1X)	Gibco	21340039
HAT Supplement (50X)	Gibco	21060017
Insulin-T ransferrin-Selenium-Ethanolamine (ITS -X) (100X)	Gibco	51500056
MEM Nonessential Amino Acids (100x)	Corning	25-025-CI
Sodium Pyruvate 100mM solution	Corning	25-000-CI
GlutaMAX Supplement	Gibco	35050061
Penicillin-Streptomycin solution (100x)	Corning	30-002-CI
DMEM high glucose medium	Millipore-Sigma	D6429
HT (Hypoxanthine, Thymidine) (50x)	Corning	25-047-CI
1-oxyl-2,2,5,5-tetramethylpyrroline-3-methyl-methanethiosulfonate (MTSSL)	Enzo LifeScience	ALX-430-134
Bicinchoninic Acid solution	Millipore-Sigma	B9643
X-tremeGENE HP DNA Transfection Reagent	Millipore-Sigma	XTGHP-RO
Polybrene Infection/Transfection Reagent	Millipore-Sigma	TR1003
EDTA-free Protease Inhibitor Cocktail	Roche	05892791001
Newborn Calf Serum (NCS)	Millipore-Sigma	N4637
Puromycin dihydrochloride	Millipore-Sigma	P8833
L-Glutamine	Gibco	25030081
Experimental models: Organisms/strains		
E. coli DH5α	GoldBio	CC-101-TR
E. coli DH10Bac	ThermoFisher	10361012
E. coli BL21 (DE3)	NEB	C2527I
HEK-293S GnTI⁻	ATCC	CRL-3022
NIH/3T3	ATCC	CRL-1658
HEK-293T	Clontech	632180
SP2-mIL6 mouse myeloma cells	ATCC	CRL-2016
Sf9 insect cell	Expression System	94-001S
Critical commercial assays		
RNEAsy Mini Kit	Qiagen	74106
Superscript III First Strand Kit	Invitrogen	18080-51
GoTaq Polymerase Kit	Promega	M3005
uMACS GFP Isolation Kit	Miltenyi Biotec	130091125
Deposited data		

REAGENT or RESOURCE	SOURCE	IDENTIFIER
Crystal structure of cystinosin-P10	This paper	PDB: 8DYP
Cryo-EM structure of cystinosin-3H5 (lumen-open)	This paper	PDB: 8DKI EMDB: 27489
Cryo-EM structure of cystinosin-3H5 (cytosol-open)	This paper	PDB: 8DKE EMDB: 27488
Cryo-EM structure of cystinosin-3H5 (cystine-bound)	This paper	PDB: 8DKM EMDB: 27490
Cryo-EM structure of cystinosin-3H5 N288K (pH5.0)	This paper	PDB: 8DKW EMDB: 27492
Cryo-EM structure of cystinosin-3H5 N288K (pH7.5)	This paper	PDB 8DKX EMDB: 27493
Recombinant DNA		
pEG-BacMam-CTNS	This paper	N/A
pEGFP-N1-CTNS	This paper	N/A
Software and algorithms		
HKL2000	Otwinowski and Minor, 1997	https://www.hkl-xray.com/
PHASER	McCoy, 2007	http://www.phaser.cimr.cam.ac.uk/
Phenix 1.19	Adams et al., 2010	http://www.phenix-online.org/
SerialEM 3.7.10	Mastronarde, 2005	http://bio3d.colorado.edu/SerialEM/
RELION 3.1	Zivanov et al., 2018	https://www2.mrc-lmb.cam.ac.uk/relion
CTFFIND4 4.1.8	Rohou and Grigorieff, 2015	http://grigoriefflab.janelia.org/ctffind4
MotionCor2 1.1.1	Li et al., 2013	https://emcore.ucsf.edu/ucsf-software
crYOLO 1.7.6	Wagner et al., 2019	https://cryolo.readthedocs.io/en/stable/
MolProbity 4.3	Chen et al., 2010b	http://molprobity.biochem.duke.edu/
COOT 0.9.6	Emsley and Cowtan, 2004	http://www2.mrc-lmb.cam.ac.uk/personal/pemsley/coot
Chimera 1.12	Pettersen et al., 2004	http://www.cgl.ucsf.edu/chimera
PyMOL 1.8	Schrodinger	http://www.pymol.org
Consurf	Landau M. et al., 2005	https://consurf.tau.ac.il
DEERAnalysis2019	Jeschke et al., 2006	https://epr.ethz.ch/software/
Prism 6.0	GraphPad	https://www.graphpad.com